SLAC–PUB–8406
CPHT–S001–0100
hep-ph/0003233

Exclusive production of pion pairs in $\gamma^*\gamma$ collisions at large Q^2 *

M. Diehl †
Stanford Linear Accelerator Center, Stanford University, Stanford, CA 94309, U.S.A.

T. Gousset
SUBATECH, B.P. 20722, 44307 Nantes, France ‡

B. Pire
CPhT, École Polytechnique, 91128 Palaiseau, France §
(March 2000)

We perform a QCD analysis of the exclusive production of two mesons in $\gamma^*\gamma$ collisions in the kinematical domain of large photon virtuality Q and small hadronic invariant mass W. This reaction is dominated by a scale invariant mechanism which factorizes into a perturbative subprocess, $\gamma^*\gamma \to q\bar{q}$ or $\gamma^*\gamma \to gg$, and a generalized two-meson distribution amplitude. We develop in detail the phenomenology of this process at e^+e^- colliders. Using a simple model for the two-pion distribution amplitude, based on its general properties, we estimate the cross section for the kinematics accessible at BABAR, BELLE, CLEO and LEP.

Submitted to Physical Review D

I. INTRODUCTION

Exclusive hadron production in two-photon collisions provides a tool to study a variety of fundamental aspects of QCD and has long been a subject of great interest (cf., e.g., [1–3] and references therein). Recently a new facet of this has been pointed out, namely the physics of the process $\gamma^*\gamma \to \pi\pi$ in the region where Q^2 is large but W^2 small [4]. This process factorizes [5,6] into a perturbatively calculable, short-distance dominated scattering $\gamma^*\gamma \to q\bar{q}$ or $\gamma^*\gamma \to gg$, and non-perturbative matrix elements measuring the transitions $q\bar{q} \to \pi\pi$ and $gg \to \pi\pi$. We have called these matrix elements generalized distribution amplitudes (GDAs) to emphasize their close connection to the distribution amplitudes introduced many years ago in the QCD description of exclusive hard processes [7].

Indeed it is instructive to consider $\gamma^*\gamma \to \pi\pi$ as a generalization of the process $\gamma^*\gamma \to \pi^0$, where the distribution amplitude of a single pion appears. The γ–π transition form factor has been the subject of detailed theoretical studies [8]. The experimental data [9] are well reproduced by a description based on QCD factorization and provide one of the best constraints so far on the form of the single-pion distribution amplitude.

From a different point of view $\gamma^*\gamma \to \pi\pi$ is the crossed channel of virtual Compton scattering on a pion. The kinematical region we consider here is closely related to deeply virtual Compton scattering (DVCS), which has attracted considerable attention in the context of skewed parton distributions [10].

Our reaction can also be seen as the exclusive limit of a hadronization process. The hadronization of a $q\bar{q}$-pair originating from a hard, short-distance process such as a $\gamma^*\gamma$ collision is usually formulated in terms of fragmentation functions which describe in a universal way semi-inclusive reactions, specifically the transition from a quark or antiquark to a final-state hadron when one integrates over all final states containing this hadron. We specialize here to the case where the final state consists of two mesons with specified four-momenta, and nothing else.

---

*Work supported by Department of Energy contract DE–AC03–76SF00515 and by TMR contracts FMRX–CT96–0008 and FMRX–CT98–0194
†Supported by the Feodor Lynen Program of the Alexander von Humboldt Foundation
‡Unité mixte 6457 de l'Université de Nantes, de l'École des Mines de Nantes et de l'IN2P3/CNRS
§Unité mixte C7644 du CNRS

Like other hadronic matrix elements the GDAs are process independent. It has recently been pointed out [11] that they occur in the hard exclusive process $\gamma^* p \to \pi\pi p$, where the pion pair is or is not the decay product of a ρ meson, and that the analysis of that reaction would benefit from the measurement of the two-pion GDA in $\gamma^*\gamma \to \pi\pi$.

All these aspects lead us to consider GDAs as a promising new tool for hadronic physics, which may be used to unveil some of the mysteries of hadronization and the confining regime of QCD. The process $\gamma^*\gamma \to \pi\pi$ is well suited to access these quantities experimentally. In the present paper, we develop in detail the phenomenology of this reaction and emphasize the feasibility of its investigation at existing e^+e^- colliders.

In Sect. II we discuss the kinematics of our process, recall its main properties in the factorization regime we are interested in, and elaborate on the crossing relation between $\gamma^*\gamma \to \pi\pi$ and deep virtual Compton scattering. In Sect. III we list the general properties of generalized distribution amplitudes and in particular give a derivation of their QCD evolution equations. These properties lead us to construct a simple model of the two-pion GDA, which is described in Sect. IV. Section V gives a comparison between one-pion and two-pion production in $\gamma^*\gamma$ collisions. Relations with the inclusive production of hadrons, commonly described by the photon structure function, are discussed in Sect. VI. The phenomenology of our process in $e\gamma$ collisions is described in detail in Sect. VII, with special emphasis on the information contained in angular distributions and in the interference with the bremsstrahlung mechanism. In Sect. VIII we give estimates for the cross section for various experimental setups at existing e^+e^- colliders. Section IX contains our conclusions. In Appendix A we specify our sign conventions for pion states, and in Appendix B we discuss what additional information can be obtained with polarized beams.

II. THE PROCESS $\gamma^*\gamma \to \pi\pi$

A. Kinematics in the $\gamma^*\gamma$ center of mass.

The reaction we are interested in is

$$e(k) + \gamma(q') \to e(k') + \pi^i(p) + \pi^j(p'), \tag{1}$$

where four-momenta are indicated in parentheses. We further use

$$q = k - k', \qquad Q^2 = -q^2, \qquad P = p + p', \qquad W^2 = P^2. \tag{2}$$

The pions may be charged ($i = +,\ j = -$) or neutral ($i = j = 0$), and the lepton e may be an electron or a positron. Scattered with large momentum transfer this lepton radiates a virtual photon $\gamma^*(q)$, and for the $\gamma^*\gamma$ subprocess we introduce the Bjorken variable

$$x = \frac{Q^2}{2q\cdot q'} = \frac{Q^2}{Q^2 + W^2}. \tag{3}$$

In e^+e^- collisions the photon $\gamma(q')$ can be obtained by bremsstrahlung from the other beam lepton, so that the overall process is

$$e(k) + e(l) \to e(k') + e(l') + \pi^i(p) + \pi^j(p') \tag{4}$$

with $q' = l - l'$. In the spirit of the equivalent photon approximation we approximate q'^2 as zero and the momenta q' and l as collinear. We write $E_1 = k^0$, $E_2 = l^0$ and $q'^0 = x_2\, l^0$ for the energies in the laboratory frame.[1] For the c.m. energies of the ee and $e\gamma$ collisions we have

$$s_{ee} = (k + l)^2, \qquad s_{e\gamma} = (k + q')^2 = x_2\, s_{ee}. \tag{5}$$

Let us now discuss the kinematics in the $\gamma^*\gamma$ center of mass frame. We use a coordinate system with the z axis along $\mathbf{q}$, and with x and y axes such that $\mathbf{p}$ lies in the x-z plane and has a positive x component, i.e.,

$$q = (q^0, 0, 0, |\mathbf{q}|), \qquad p = (p^0, |\mathbf{p}|\sin\theta, 0, |\mathbf{p}|\cos\theta), \tag{6}$$

[1] We neglect the small finite crossing angle between the beams at BELLE, so that in our parlance the lepton beams are collinear in the "laboratory frame".

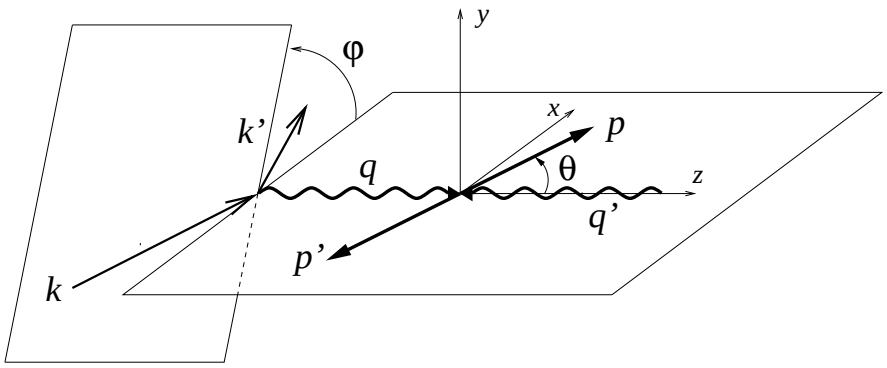

FIG. 1. The kinematics of $e(k)+\gamma(q')\to e(k')+\pi^i(p)+\pi^j(p')$ in the center of mass of the pion pair.

where we have introduced the polar angle θ of $\mathbf{p}$. Another natural variable for our process in this frame is the azimuth φ of $\mathbf{k}'$, which is the angle between the leptonic and the hadronic planes, cf. Fig. 1. In terms of Lorentz invariants these angles can be obtained from

$$\begin{aligned}
\cos\theta &= \frac{2q\cdot(p'-p)}{\beta\,(Q^2+W^2)},\\
\cos\varphi &= \frac{2k\cdot(p'-p)\,(Q^2+W^2)+\beta\cos\theta\,[Q^2(s_{e\gamma}-Q^2-W^2)-s_{e\gamma}W^2]}{2\beta\sin\theta\sqrt{s_{e\gamma}\,Q^2W^2(s_{e\gamma}-Q^2-W^2)}},\\
\sin\varphi &= \frac{4\epsilon_{\alpha\beta\gamma\delta}\,(p+p')^\alpha\,p^\beta\,k^\gamma\,q^\delta}{\beta\sin\theta\sqrt{s_{e\gamma}\,Q^2W^2(s_{e\gamma}-Q^2-W^2)}}
\end{aligned} \tag{7}$$

with $\epsilon_{0123}=+1$ and the velocity

$$\beta=\sqrt{1-\frac{4m_\pi^2}{W^2}} \tag{8}$$

of the pions. A further quantity we will use is the usual y-variable for the $e\gamma$ collision,

$$y=\frac{q\cdot q'}{k\cdot q'}=\frac{Q^2+W^2}{s_{e\gamma}}, \tag{9}$$

which can be traded for

$$\epsilon=\frac{1-y}{1-y+y^2/2}, \tag{10}$$

the ratio of longitudinal to transverse polarization of the virtual photon $\gamma^*(q)$.

We finally define light cone components $a^\pm=(a^0\pm a^3)/\sqrt{2}$ for any four-vector a and introduce the fraction

$$\zeta=\frac{p^+}{P^+}=\frac{1+\beta\cos\theta}{2} \tag{11}$$

of light cone momentum carried by $\pi^i(p)$ with respect to the pion pair.

B. Factorization at large Q^2 and small W^2

Let us briefly review how $\gamma^*\gamma\to\pi\pi$ factorizes in the kinematical regime we are interested in. Firstly, we require Q^2 to be large compared with the scale $\Lambda^2\sim 1$ GeV^2 of soft interactions, thus providing a hard scale for the process. Secondly, we ask W^2 to be small compared with this large scale Q^2. In this regime the dynamics of the process is conveniently represented in the Breit frame, obtained by boosting from the $\gamma^*\gamma$ center of mass along z. The spacetime cartoon of the process one can derive from power counting and factorization arguments is shown in Fig. 2.

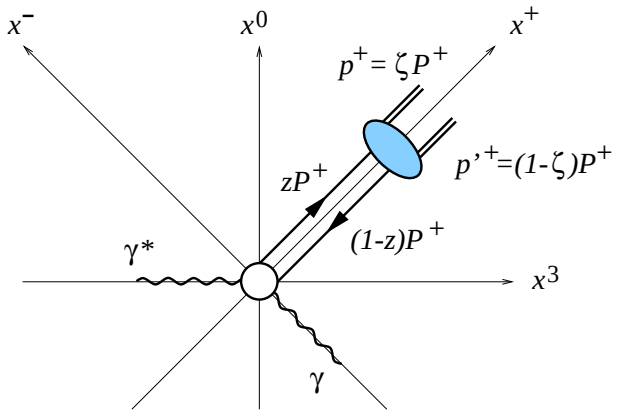

FIG. 2. Spacetime diagram of $\gamma^*\gamma \to \pi\pi$ in the Breit frame.

In the Breit frame the real photon moves fast along $-z$ and is scattered into an energetic hadronic system moving along $+z$. The hard part of this process takes place at the level of elementary constituents, and the minimal number of quarks and gluons compatible with conservation laws (color etc.) are produced. At Born level one simply has $\gamma^*\gamma \to q\bar{q}$, but through a quark box the photons can also couple to two gluons. Each quark or gluon carries a fraction z or $1-z$ of the large light-cone momentum component P^+. Subsequently the soft part of the reaction, i.e., hadronization into a pion pair, takes place.

At leading order in α_S the amplitude is given by the diagram of Fig. 3 (a) and the one where the two photon vertices are interchanged. One calculates for the hadronic tensor [4]

$$T^{\mu\nu} = i \int d^4x\, e^{-iq\cdot x} \,\langle \pi(p)\pi(p')|\, T J^{\mu}_{\rm em}(x) J^{\nu}_{\rm em}(0)\,|0\rangle = -g_T^{\mu\nu} \sum_q \frac{e_q^2}{2} \int_0^1 dz\, \frac{2z-1}{z(1-z)}\, \Phi_q^{\pi\pi}(z,\zeta,W^2), \tag{12}$$

where $g_T^{\mu\nu}$ denotes the metric tensor in transverse space ($g^{11} = -1$). The sum on the r.h.s. runs over all quarks flavors, e_q is the charge of quark q in units of the positron charge e, and $eJ^{\mu}_{\rm em}(x)$ is the electromagnetic current. While the expression of the hard subprocess $\gamma^*\gamma \to q\bar{q}$ is explicit in Eq. (12), the soft part of $\gamma^*\gamma \to \pi\pi$ is parameterized by the generalized distribution amplitude

$$\Phi_q^{\pi\pi}(z,\zeta,W^2) = \int \frac{dx^-}{2\pi} e^{-iz(P^+x^-)} \,\langle \pi(p)\pi(p')|\, \bar{q}(x^-)\gamma^+ q(0)\,|0\rangle \tag{13}$$

for each quark flavor q. We work in light cone gauge $A^+ = 0$, otherwise the usual path ordered exponential of gluon potentials appears between the quark fields. Φ_q depends on the light-cone fraction z of the quark with respect to the pion pair, on the kinematical variables ζ and W^2 of the pions, and on a factorization scale. The latter dependence, not displayed in Eq. (13), will be discussed in Sect. III B.

In Eq. (12) a scaling behavior for our process is manifest: at fixed ζ and W^2 the $\gamma^*\gamma$ amplitude is independent of Q^2, up to logarithmic scaling violations from radiative corrections to the hard scattering and from the evolution of the two-pion distribution amplitude. This scaling property is central to all processes where a factorization theorem holds, and it is the basic signature one looks for when testing whether the asymptotic analysis developed here applies to an experimental situation at finite Q^2. There will of course be power corrections in Λ/Q and W/Q to this leading mechanism. Examples are the hadronic component of the real photon, and the effect in the hard scattering of the transverse momentum of the produced parton pair. We note that the crossed channel, i.e., virtual Compton scattering has been analyzed in detail within the operator product expansion [5,12,13], which provides a framework for a systematic study of higher twist effects.

Contracting the hadronic tensor (12) with the photon polarization vectors we see that in order to give a nonzero $\gamma^*\gamma \to \pi\pi$ amplitude the virtual photon must have the same helicity as the real one. As in the case of deep virtual Compton scattering this is a direct consequence of chiral invariance in the collinear hard-scattering process [14,15] and is valid at all orders in α_S. In the case of the $\gamma^*\gamma \to gg$ subprocess the photon helicities can also be opposite [16]. In any case the virtual photon must be transverse. As a consequence nonleading twist effects can be studied in the amplitude for longitudinal γ^* polarization, without any "background" from leading twist pieces. We will develop in Sect. VII how the different $\gamma^*\gamma$ helicity amplitudes are experimentally accessible.

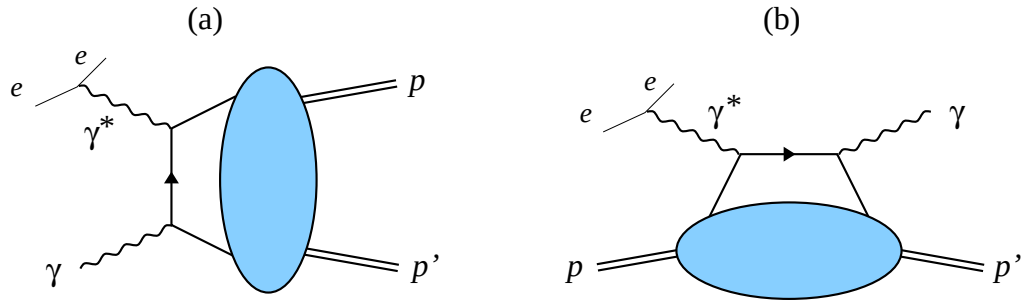

FIG. 3. (a) Factorization of the process $\gamma^*\gamma \to \pi\pi$ in the region $Q^2 \gg W^2, \Lambda^2$. The hard scattering is shown at Born level, with a second diagram being obtained by interchanging the two photon vertices. The blob denotes the two-pion GDA. (b) Crossing relates this process to deep virtual Compton scattering, $\gamma^*\pi \to \gamma\pi$. The blob now denotes the (skewed) quark distribution in the pion.

As we already mentioned, there is a close analogy of two-pion production in the region $Q^2 \gg W^2, \Lambda^2$ with the one-pion channel, commonly described in terms of the γ–π transition form factor. There again a factorization theorem holds, which allows the hadronic tensor $T^{\mu\nu}$ to be expressed in terms of the single-pion distribution amplitude ϕ^π as

$$T^{\mu\nu} = i \int d^4x\, e^{-iq\cdot x} \,\langle \pi^0 |\, T J^\mu_{\rm em}(x) J^\nu_{\rm em}(0)\, |0\rangle = \epsilon_T^{\mu\nu} \sum_q \frac{e_q^2}{2} \int_0^1 dz\, \frac{1}{z(1-z)}\, \phi_q^\pi(z) \tag{14}$$

to leading order in α_S, where $\epsilon_T^{\mu\nu}$ is the antisymmetric tensor in transverse space ($\epsilon_T^{12} = 1$) and

$$\phi_q^\pi(z) = i \int \frac{dx^-}{2\pi} e^{-iz(P^+x^-)} \,\langle \pi^0(P) |\, \bar q(x^-)\gamma^+\gamma_5\, q(0)\, |0\rangle. \tag{15}$$

Notice the different Dirac structures in the matrix elements (13) and (15), due to the different parity transformation properties of one- and two-pion states [4].

The theoretical analysis of this process has been highly developed [8]. Its generalization to the production of η and η' is also important, in particular with respect to the $SU(3)$ flavor structure of the QCD evolution equations and the mixing of the quark singlet and gluon channels [17]. In Sect. V we will further compare the production of a single pion with that of a pion pair.

C. Relation with deep virtual Compton scattering and parton distributions in the pion

The process $\gamma^*\gamma \to \pi\pi$ at large Q^2 and $s \ll Q^2$ is related by s–t crossing to deep virtual Compton scattering on a pion, i.e., to $\gamma^*\pi \to \gamma\pi$ at large Q^2 and $-t \ll Q^2$. It turns out that factorization works in completely analogous ways for both cases, as is shown in Fig. 3. The non-perturbative matrix elements occurring in the Compton process are skewed parton distributions [10], defined in the pion case as [18]

$$H_q(x,\xi,t) = \frac{1}{2} \int \frac{dz^-}{2\pi}\, e^{ix(P^+z^-)} \,\langle \pi(p') | \bar q(-z^-/2)\gamma^+ q(z^-/2) | \pi(p)\rangle \tag{16}$$

with $P = (p+p')/2$. They have been recognized as objects of considerable interest and have triggered intensive theoretical and experimental work. The processes $\gamma^*\gamma \to \pi\pi$ and $\gamma^*\pi \to \gamma\pi$ share many common features, from their scaling behavior and the details of their helicity selection rules to the possibilities of phenomenological analysis, which we will develop in Sect. VII.

The imaginary part of the forward virtual Compton amplitude, $\gamma^*\pi \to \gamma^*\pi$, obtained from Fig. 3 (b) by replacing the γ with a second γ^*, gives the cross section for inclusive deep inelastic scattering, $\gamma^*\pi \to X$, where the ordinary parton distributions in a pion occur.

As observed in [18] it is useful to implement crossing at the level of moments in momentum fractions (z and ζ for GDAs, x and ξ for SPDs), which depend only on a factorization scale and a Lorentz invariant (s for GDAs, t for SPDs). The moments of GDAs and of SPDs are connected by analytic continuation in that invariant. In particular, analytic continuation to the point $t = 0$ leads to moments of the ordinary parton distributions in the pion, which we will use as an input for our model of GDAs in Sect. IV.

III. GENERAL PROPERTIES OF GDAS

A. Charge conjugation and isospin properties

Let us start by compiling some symmetry properties which will be useful in the following. For the quark GDAs (13) the invariance of strong interactions under charge conjugation C implies

$$\Phi_q^{\pi\pi}(z,\zeta,W^2) = -\Phi_q^{\pi\pi}(1-z,1-\zeta,W^2). \tag{17}$$

It is useful to project GDAs for charged pions on eigenstates of C parity,

$$\Phi_q^{\pm}(z,\zeta,W^2) = \frac{1}{2}\left(\Phi_q^{\pi^+\pi^-}(z,\zeta,W^2) \pm \Phi_q^{\pi^+\pi^-}(z,1-\zeta,W^2)\right), \tag{18}$$

so that

$$\Phi_q^{\pi^+\pi^-} = \Phi_q^{+}(z,\zeta,W^2) + \Phi_q^{-}(z,\zeta,W^2). \tag{19}$$

In the C even sector Eq. (17) reduces to

$$\Phi_q^{+}(z,\zeta,W^2) = -\Phi_q^{+}(1-z,\zeta,W^2). \tag{20}$$

Our process is only sensitive to the C even part of $\Phi_q^{\pi^+\pi^-}$ since the initial state two-photon state has positive C parity. Of course a $\pi^0\pi^0$ pair has positive C parity as well, so that $\Phi_q^{\pi^0\pi^0}$ has no C-odd part at all.

Let us now turn to isospin symmetry. The C odd component of a two-pion state has total isospin $I=1$, whereas its C even component contains both $I=0$ and $I=2$ pieces. The quark operator in $\Phi_q^{\pi\pi}$ has only components with isospin $I=0$ or $I=1$. Hence it is a consequence of the leading twist production mechanism and of isospin invariance that in our process the pion pair is in a state of zero isospin, i.e., that no component with $I=2$ is produced. Another consequence of isospin invariance is that

$$\Phi_q^{\pi^0\pi^0}(z,\zeta,W^2) = \Phi_q^{+}(z,\zeta,W^2), \tag{21}$$

so that the production amplitudes for neutral and charged pion pairs are equal. Deviations from isospin symmetry in the present reaction would be interesting, but since one can expect them to be small we will assume isospin invariance to hold throughout the rest of our study. Isospin invariance also implies that

$$\Phi_u^{+} = \Phi_d^{+}, \qquad \Phi_u^{-} = -\Phi_d^{-}, \tag{22}$$

so that in the C even sector we only need to know the $SU(2)$ flavor singlet combination $\Phi_u^+ + \Phi_d^+$.

The connection between the notation $\Phi_{||}^{I=0,1}$ of Polyakov [19] and ours is

$$\Phi_{||}^{I=0} = \Phi_u^{+}, \qquad \Phi_{||}^{I=1} = \Phi_u^{-}. \tag{23}$$

We remark that the second term in Eq. (2.6) of Ref. [19] should come with a minus sign [20]. Our relation $\Phi_{||}^{I=1} = \Phi_u^-$ takes this correction into account.

Notice that the signs in Eqs. (21) and (23) depend on the choice of relative phases in the definition of charged pion states. We specify our convention in Appendix A.

B. Evolution equation

In the process of factorization generalized distribution amplitudes acquire a scale dependence in the same way as usual distributions do. This scale dependence can be computed within perturbative QCD, and there is nothing special with multiparticle states since the scale dependence is a property of the nonlocal product of fields under consideration, rather than one of a particular hadronic matrix element (see [21] for an approach exploiting this feature). The scale dependence of GDAs can be cast in the form of an ERBL evolution equation [22], and the only complication in the C even channel we are concerned with here is the mixing of quark and gluon distribution amplitudes [23]. The leading-logarithmic form of the evolution equations has been derived in Ref. [17] for the parity-odd sector, where the relevant quark operator is $\bar{q}\gamma^+\gamma_5\, q$. Our application to pion pairs leads us to consider the parity-even sector, cf. our

remark after Eq. (15), and we will now give the basic steps for deriving the evolution equation, following the procedure outlined in [17].

We are then concerned with the generalized quark and gluon distribution amplitudes in $A^+ = 0$ gauge:

$$\begin{aligned}
\Phi_q(z,\zeta,W^2) &= \int \frac{dx^-}{2\pi}\, e^{-iz(P^+x^-)} \langle \pi(p)\pi(p')|\bar{q}(x^-)\gamma^+ q(0)|0\rangle, \\
\Phi_g(z,\zeta,W^2) &= \frac{1}{P^+}\int \frac{dx^-}{2\pi}\, e^{-iz(P^+x^-)} \langle \pi(p)\pi(p')|F^{+\mu}(x^-)F_\mu{}^+(0)|0\rangle, \\
&= z(1-z)P^+ \int \frac{dx^-}{2\pi}\, e^{-iz(P^+x^-)} \langle \pi(p)\pi(p')|A^\mu(x^-)A_\mu(0)|0\rangle.
\end{aligned} \tag{24}$$

Our gluon distribution amplitude $\Phi_g(z,\zeta,W^2)$ coincides with $\Phi^G(z,\zeta,W^2)$ introduced in [16]. From the definition (24) one readily obtains

$$\Phi_g(z,\zeta,W^2) = \Phi_g(1-z,\zeta,W^2), \tag{25}$$

and from C invariance one has

$$\Phi_g(z,\zeta,W^2) = \Phi_g(1-z,1-\zeta,W^2). \tag{26}$$

Here we have given definitions for a two-pion state, but as stated above the evolution equation for DAs and GDAs is not specific to the details of the hadronic system. The considerations of this and the following subsection thus apply to any state in the parity even sector which has four-momentum P and total angular momentum $J_z = 0$ along the axis defining the light cone variables.

We now study the evolution of the distributions for gluons and of quarks in the singlet combination of n_f flavors. For convenience we introduce

$$z\bar{z}\, f_Q(z) = \sum_{q=1}^{n_f} \Phi_q(z), \tag{27}$$

$$z^2\bar{z}^2\, f_G(z) = \Phi_g(z), \tag{28}$$

where we use the notation $\bar{z} = 1 - z$. In the end we will return to the amplitudes Φ_q and Φ_g.

The scale dependence is controlled by the parameter

$$\xi(\mu^2,\mu_0^2) = \frac{2}{\beta_1} \ln\left(\frac{\alpha_S(\mu_0^2)}{\alpha_S(\mu^2)}\right), \tag{29}$$

where α_S is the one-loop running coupling and $\beta_1 = 11 - 2n_f/3$. This parameter describes how the distribution amplitude evolves when one changes the factorization point from μ_0 to μ. The evolution equation takes the form

$$\frac{\partial}{\partial\xi} f(z,\xi) = V * f = \int_0^1 du\, V(z,u)\, f(u,\xi). \tag{30}$$

where f is a two-component vector

$$f = \begin{pmatrix} f_Q \\ f_G \end{pmatrix}, \tag{31}$$

and V is the 2×2 matrix kernel

$$V = \begin{pmatrix} V_{QQ} & V_{QG} \\ V_{GQ} & V_{GG} \end{pmatrix}. \tag{32}$$

To obtain the leading logarithmic evolution equation it is sufficient to consider one-loop corrections to the scattering amplitude. The latter is depicted in Fig. 4 and has the form $H * f$, where $H = (H_Q, H_G)$ denotes the hard-scattering kernels. It turns out that in light cone gauge $A^+ = 0$ the relevant one-loop diagrams consist of an insertion between H and f of the graphs shown in Fig. 5 (a) to (e), supplemented by (renormalized) self-energy insertions on each line connecting H to f in Fig. 4. Calling the sum of these insertions ξV the one-loop diagrams have the structure $H * \xi V * f$.

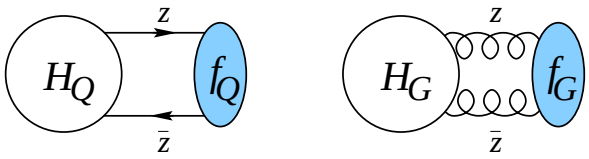

FIG. 4. The scattering amplitude $H * f$ with f denoting the soft matrix elements and H the hard scattering kernels.

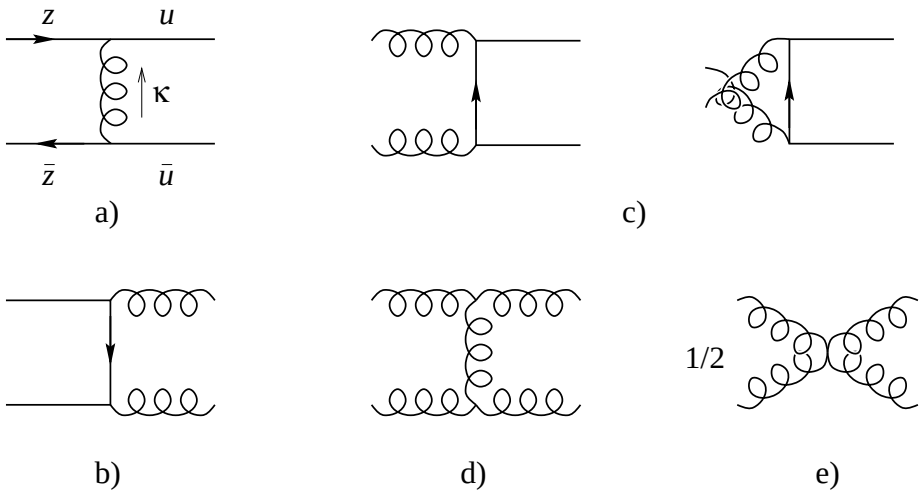

FIG. 5. One-loop insertions, to be supplemented by self-energy insertions on every line appearing in Fig. 4. The sum of all insertions gives the evolution kernel ξV. We remark that the one-loop graph (e) must be multiplied by 1/2 to avoid double counting. u and z denote light cone plus momentum fractions, and κ the loop four-momentum.

The evolution from zeroth to first order of the generalized distribution amplitude may thus be written as

$$f^{(1)}(z) = f^{(0)}(z) + \xi \int_0^1 du\, V(z,u)\, f^{(0)}(u). \tag{33}$$

In the computation of the diagrams, the κ^- integral is performed by the Cauchy method of contour integration in the complex plane, and ξ is the result of the integral over transverse momentum from $\kappa_T = \mu_0$ to $\kappa_T = \mu$:

$$\xi(\mu^2, \mu_0^2) = \int_{\mu_0^2}^{\mu^2} \frac{d\kappa_T^2}{\kappa_T^2} \frac{\alpha_S(\kappa_T^2)}{2\pi}. \tag{34}$$

Despite the presence of α_S in Eq. (34), ξ is not small if $\mu^2 \gg \mu_0^2$, and this signals the necessity of an all-order analysis. This analysis leads to the evolution equation, with the feature that V is the same matrix in Eqs. (30) and (33). We refer the reader to the literature for a general discussion [24].

The integration over κ^+ may be reexpressed as an integral over the incoming light cone fraction u. The evolution kernels contain the remaining part of the dynamics, in particular they describe the change of light cone fractions from u to z. We get

$$\begin{aligned}
V_{QQ}(z,u) &= C_F \left[\theta(z-u)\frac{u}{z}\left(1+\frac{1}{z-u}\right) + \{u \leftrightarrow \bar{u},\, z \leftrightarrow \bar{z}\}\right]_+ , \\
V_{QG}(z,u) &= 2 n_f T_F \left[\theta(z-u)\frac{u}{z}(2z-u) - \{u \leftrightarrow \bar{u},\, z \leftrightarrow \bar{z}\}\right], \\
V_{GQ}(z,u) &= \frac{C_F}{z\bar{z}} \left[\theta(z-u)\frac{u}{z}(\bar{z}-2\bar{u}) - \{u \leftrightarrow \bar{u},\, z \leftrightarrow \bar{z}\}\right], \\
V_{GG}(z,u) &= \frac{C_A}{z\bar{z}} \left[\theta(z-u)\left(\frac{u\bar{u}}{z-u} - u\bar{u} - \frac{u}{2z}[(2z-1)^2 + (2u-1)^2]\right) + \{u \leftrightarrow \bar{u},\, z \leftrightarrow \bar{z}\}\right]_+ - \frac{2}{3} n_f T_F\, \delta(u-z),
\end{aligned} \tag{35}$$

where the color factors are $C_F = 4/3$, $T_F = 1/2$ and $C_A = 3$. The subscript + stands for the + distributions, whose action on a function f may be expressed symbolically as

$$[\cdots]_+ f(u) = [\cdots]\,(f(u) - f(z)). \tag{36}$$

The kernels (35) give the finite parts that remain after the cancellation of infrared divergences between graph (a), resp. (d), and quark self-energy, resp. gluon self-energy insertions. A simple way to obtain self-energy corrections is to notice their relation to parton splitting [17], that is

$$\begin{aligned} f_Q^{(1)}(z)\Big|_{SE} &= \left[1 - \xi \int dx\, P_{QQ}(x)\right] f_Q^{(0)}(z) = \left[1 - \xi \int dx\, P_{GQ}(x)\right] f_Q^{(0)}(z) \\ f_G^{(1)}(z)\Big|_{SE} &= \left[1 - \xi \int dx \left(\frac{1}{2} P_{GG}(x) + n_f P_{QG}(x)\right)\right] f_G^{(0)}(z), \end{aligned} \tag{37}$$

with the unregularized DGLAP splitting functions

$$\begin{aligned} P_{QQ}(x) &= C_F \frac{1+x^2}{1-x}, \\ P_{QG}(x) &= T_F \left[x^2 + (1-x)^2\right], \\ P_{GQ}(x) &= C_F \frac{1+(1-x)^2}{x}, \\ P_{GG}(x) &= 2\, C_A \left[\frac{x}{1-x} + \frac{1-x}{x} + x(1-x)\right]. \end{aligned} \tag{38}$$

The integrals (37) are not defined in the limit $x \to 0, 1$, which is a manifestation of the infrared divergence of self-energy graphs.

C. Solution

We will now solve the evolution equation (30). Given our application we restrict ourselves to the C even parts Φ_q^+ of the quark distributions, the gluon distribution being of course even under C from the start.

We look for solutions of the form

$$f(z, \xi) = f(z)\, e^{-\gamma \xi}. \tag{39}$$

To this end it is convenient to change variables, introducing $y = 2u - 1$ and $x = 2z - 1$, and to study the convolution of the matrix kernel V with

$$\begin{pmatrix} x^n \\ 0 \end{pmatrix}, \qquad \begin{pmatrix} 0 \\ x^{n-1} \end{pmatrix}, \tag{40}$$

where n is an odd integer to accommodate the symmetry properties (20) and (25). One finds

$$\begin{aligned} V_{QQ} * y^n &= -\gamma_{QQ}(n)\, x^n + O(x^{n-2}), & V_{QG} * y^{n-1} &= -\gamma_{QG}(n)\, x^n + O(x^{n-2}), \\ V_{GQ} * y^n &= -\gamma_{GQ}(n)\, x^{n-1} + O(x^{n-3}), & V_{GG} * y^{n-1} &= -\gamma_{GG}(n)\, x^{n-1} + O(x^{n-3}), \end{aligned} \tag{41}$$

with anomalous dimensions

$$\begin{aligned} \gamma_{QQ}(n) &= C_F \left(\frac{1}{2} - \frac{1}{(n+1)(n+2)} + 2 \sum_{k=2}^{n+1} \frac{1}{k}\right), \\ \gamma_{QG}(n) &= -n_f T_F \frac{n^2+3n+4}{n(n+1)(n+2)}, \\ \gamma_{GQ}(n) &= -2 C_F \frac{n^2+3n+4}{(n+1)(n+2)(n+3)}, \\ \gamma_{GG}(n) &= C_A \left(\frac{1}{6} - \frac{2}{n(n+1)} - \frac{2}{(n+2)(n+3)} + 2 \sum_{k=2}^{n+1} \frac{1}{k}\right) + \frac{2}{3} n_f T_F. \end{aligned} \tag{42}$$

Since for a given n_0 the space of solutions with $n \leq n_0$ is stable under the application of the kernel one can find polynomials $p_n(x)$ and $q_{n-1}(x)$ satisfying

$$\begin{aligned} V_{QQ} * p_n &= -\gamma_{QQ}(n)\, p_n, \qquad & V_{QG} * q_{n-1} &= -\gamma_{QG}(n)\, p_n, \\ V_{GQ} * p_n &= -\gamma_{GQ}(n)\, q_{n-1}, \qquad & V_{GG} * q_{n-1} &= -\gamma_{GG}(n)\, q_{n-1}. \end{aligned} \tag{43}$$

The symmetry properties of the kernels

$$\begin{aligned} (1-x^2)\, V_{QQ}(x,y) &= (1-y^2)\, V_{QQ}(y,x), \\ 2C_F(1-x^2)\, V_{QG}(x,y) &= n_f T_F (1-y^2)^2\, V_{GQ}(y,x), \\ (1-x^2)^2\, V_{GG}(x,y) &= (1-y^2)^2\, V_{GG}(y,x), \end{aligned} \tag{44}$$

then imply that the (p_n) are orthogonal polynomials on the interval $[-1,\, 1]$ with weight $1-x^2$, i.e., they are proportional to the Gegenbauer polynomials $C_n^{(3/2)}(x)$, whereas the (q_{n-1}) are orthogonal on $[-1,\, 1]$ with weight $(1-x^2)^2$, that is, proportional to the Gegenbauer polynomials $C_{n-1}^{(5/2)}(x)$. To complete the identification it is necessary to take into account the standard normalization of Gegenbauer polynomials. One finds that $p_n = C_n^{(3/2)}$ and $q_{n-1} = C_{n-1}^{(5/2)}$ fulfill Eq. (43), provided one makes the replacements

$$\gamma_{QG}(n) \to \gamma'_{QG}(n) = \frac{n}{3}\,\gamma_{QG}(n), \qquad \gamma_{GQ}(n) \to \gamma'_{GQ}(n) = \frac{3}{n}\,\gamma_{GQ}(n). \tag{45}$$

The final step is to diagonalize the 2×2 anomalous dimension matrices for each value of n. The eigenvalues are

$$\Gamma_n^{(\pm)} = \frac{1}{2}\left[\, \gamma_{QQ}(n) + \gamma_{GG}(n) \pm \sqrt{[\gamma_{QQ}(n) - \gamma_{GG}(n)]^2 + 4\gamma'_{QG}(n)\gamma'_{GQ}(n)}\, \right], \tag{46}$$

and the eigenvectors of the kernel matrix read

$$v_n^{(\pm)}(x) = \begin{pmatrix} C_n^{(3/2)}(x) \\ g_n^{(\pm)}\, C_{n-1}^{(5/2)}(x) \end{pmatrix}, \tag{47}$$

where

$$g_n^{(\pm)} = \frac{\Gamma_n^{(\pm)} - \gamma_{QQ}(n)}{\gamma'_{QG}(n)}. \tag{48}$$

The general C even solution of Eq. (30) may then be written as

$$f(x,\xi) = \sum_{\text{odd } n} \left\{ A_n^{(+)} v_n^{(+)}(x)\, e^{-\Gamma_n^{(+)}\xi} + A_n^{(-)} v_n^{(-)}(x)\, e^{-\Gamma_n^{(-)}\xi} \right\} \tag{49}$$

with integration constants $A_n^{(\pm)}$.

We now return to the amplitudes Φ_q, Φ_g and explicitly express ξ in terms of μ and μ_0. The key result of this section then reads

$$\begin{aligned} \sum_{q=1}^{n_f} \Phi_q^+(z,\mu^2) &= z(1-z) \sum_{\text{odd } n} A_n(\mu^2)\, C_n^{(3/2)}(2z-1), \\ \Phi_g(z,\mu^2) &= z^2(1-z)^2 \sum_{\text{odd } n} A'_n(\mu^2)\, C_{n-1}^{(5/2)}(2z-1), \end{aligned} \tag{50}$$

with

$$\begin{aligned} A_n(\mu^2) &= A_n^{(+)} \left(\frac{\alpha_S(\mu^2)}{\alpha_S(\mu_0^2)}\right)^{K_n^{(+)}} + A_n^{(-)} \left(\frac{\alpha_S(\mu^2)}{\alpha_S(\mu_0^2)}\right)^{K_n^{(-)}}, \\ A'_n(\mu^2) &= g_n^{(+)} A_n^{(+)} \left(\frac{\alpha_S(\mu^2)}{\alpha_S(\mu_0^2)}\right)^{K_n^{(+)}} + g_n^{(-)} A_n^{(-)} \left(\frac{\alpha_S(\mu^2)}{\alpha_S(\mu_0^2)}\right)^{K_n^{(-)}}, \end{aligned} \tag{51}$$

and exponents $K_n^{(\pm)} = 2\Gamma_n^{(\pm)}/\beta_1$, which are positive except for $K_1^{(-)} = 0$. For $n_f = 2, 3, 4$, one explicitly finds

$$K_1^{(+)} = \frac{32 + 6n_f}{99 - 6n_f} = 0.51,\ 0.62,\ 0.75, \qquad K_3^{(-)} = 0.71,\ 0.76,\ 0.82, \qquad K_3^{(+)} = 1.45,\ 1.64,\ 1.85. \tag{52}$$

From Eq. (51) we easily see that the integration constants $A_n^{(\pm)}$ depend on the starting scale μ_0 of the evolution through a factor $\alpha_S(\mu_0^2)^{K_n^{(\pm)}}$.

D. Expansion in ζ

For a two-meson state, the coefficients A_n and A'_n are functions of the factorization scale μ^2 and of the remaining kinematical variables ζ and W^2. From the definition of GDAs in term of fields given in Eq. (24) one obtains moments

$$\begin{aligned}
\int_0^1 dz\, z^n\, \Phi_q(z) &= \frac{1}{(P^+)^{n+1}} \Big[(-i\partial^+)^n \langle \pi(p)\pi(p')|\, \bar q(x)\gamma^+ q(0)\, |0\rangle\Big]_{x=0}, \\
\int_0^1 dz\, z^{n-1}\, \Phi_g(z) &= \frac{1}{(P^+)^{n+1}} \Big[(-i\partial^+)^{n-1} \langle \pi(p)\pi(p')|\, F^{+\mu}(x) F_\mu{}^+(0)\, |0\rangle\Big]_{x=0}.
\end{aligned} \tag{53}$$

These local matrix elements are the plus-components of tensors that can be decomposed on a basis built up with the metric $g^{\mu\nu}$ and the vectors $(p+p')^\mu$ and $(p-p')^\mu$. Since $(p+p')^+ = P^+$ and $(p-p')^+ = (2\zeta - 1)P^+$ the moments (53) are then polynomials in $2\zeta - 1$ with degree at most $n+1$. The A_n and A'_n are Gegenbauer moments of $\sum_q \Phi_q$ and Φ_g, respectively, and therefore have the same polynomiality properties in ζ. Following [19] we expand them on the Legendre polynomials, writing

$$A_n(\zeta, W^2) = 6n_f \sum_{\text{even } l}^{n+1} B_{nl}(W^2)\, P_l(2\zeta - 1) \tag{54}$$

and the analogous expression for A'_n with coefficients B'_{nl}. The C invariance properties (17) and (26) restrict l to even integers in the C even sector. The expansion coefficients B_{nl} are linear combinations of the local operator matrix elements in Eq. (53) and are therefore analytic functions in W^2. As we mentioned in Sect. II C their continuation to zero or spacelike W^2 leads to the moments of parton distributions in the pion.

From Eq. (51) the factorization scale dependence of the B_{nl} may be written as

$$B_{nl}(W^2, \mu^2) = B_{nl}^{(+)}(W^2) \left(\frac{\alpha_S(\mu^2)}{\alpha_S(\mu_0^2)}\right)^{K_n^{(+)}} + B_{nl}^{(-)}(W^2) \left(\frac{\alpha_S(\mu^2)}{\alpha_S(\mu_0^2)}\right)^{K_n^{(-)}}, \tag{55}$$

with an analogous equation for B'_{nl} involving the factors $g_n^{(\pm)}$.

In the limit $\mu \to \infty$ only the terms with the smallest exponent $K_1^{(-)} = 0$ in the coefficients (51) survive. The asymptotic form of the distribution amplitudes thus has only $n = 1$ in the Gegenbauer expansion (50) and reads

$$\begin{aligned}
\sum_{q=1}^{n_f} \Phi_q^+(z, \zeta, W^2) &= 18 n_f z(1-z)(2z-1)\, \Big[B_{10}^{(-)}(W^2) + B_{12}^{(-)}(W^2)\, P_2(2\zeta - 1)\Big], \\
\Phi_g(z, \zeta, W) &= 48 z^2(1-z)^2\, \Big[B_{10}^{(-)}(W^2) + B_{12}^{(-)}(W^2)\, P_2(2\zeta - 1)\Big],
\end{aligned} \tag{56}$$

where $P_2(2\zeta - 1) = 1 - 6\zeta(1-\zeta)$. Note that $B_{10}^{(-)}$ and $B_{12}^{(-)}$ do not depend on a starting scale μ_0 because $K_1^{(-)} = 0$. For reasons that will become clear we will also keep the terms with the first nonzero exponent $K_1^{(+)}$ in our model for the GDAs to be developed in Sect. IV. For the quark distribution amplitudes this simply amounts to replacing $B_{10}^{(-)}$ and $B_{12}^{(-)}$ in the first line of Eq. (56) with the μ-dependent coefficients B_{10} and B_{12}.

Let us finally remark that, as discussed in [16], there is another generalized gluon distribution amplitude, with an operator different from the one in Eq. (24). It corresponds to pion pairs with angular momentum $J_z = \pm 2$ and gives the leading-twist part of the amplitudes $\gamma^*\gamma \to \pi\pi$ where the photon helicities are opposite. The evolution of this helicity-two distribution amplitude does not mix with any quark distribution. Its smallest anomalous dimension is positive, so that this distribution amplitude tends logarithmically to zero as $\mu \to \infty$. The study of this distribution would be very interesting. Nothing is, however, known about its size at present, and in our phenomenological analysis we will neglect its contribution.

E. Partial wave expansion

The decomposition of generalized distribution amplitudes on Legendre polynomials performed in the previous section translates into a partial waves decomposition [19] if one transforms from polynomials $P_l(2\zeta-1)$ to $P_l(\cos\theta)$ using that $2\zeta-1=\beta\cos\theta$. The rearranged series reads

$$\sum_{q=1}^{n_f}\Phi_q^+ = 6n_f\, z(1-z)\sum_{\substack{n=1\\ \text{odd}}}^{\infty}\sum_{\substack{l=0\\ \text{even}}}^{n+1}\tilde B_{nl}(W^2)\, C_n^{(3/2)}(2z-1)\, P_l(\cos\theta) \tag{57}$$

for quarks, where the coefficients $\tilde B_{nl}(W^2)$ are linear combinations of the form

$$\tilde B_{nl} = \beta^l\,\left[B_{nl} + c_{l,\,l+2}\, B_{n,\,l+2} + \ldots + c_{l,\,n+1}\, B_{n,\,n+1}\right] \tag{58}$$

with polynomials $c_{l,\,l'}$ in β^2. Keeping only $n=1$ in the Gegenbauer expansion one is restricted to an S- and a D-wave:

$$\begin{aligned}\sum_{q=1}^{n_f}\Phi_q^+ &= 18n_f\, z(1-z)(2z-1)\left[B_{10}(W^2) + B_{12}(W^2)\, P_2(2\zeta-1)\right]\\ &= 18n_f\, z(1-z)(2z-1)\left[\tilde B_{10}(W^2) + \tilde B_{12}(W^2)\, P_2(\cos\theta)\right]\end{aligned} \tag{59}$$

with

$$\begin{aligned}\tilde B_{10}(W^2) &= B_{10}(W^2) - \frac{1-\beta^2}{2}B_{12}(W^2),\\ \tilde B_{12}(W^2) &= \beta^2 B_{12}(W^2).\end{aligned} \tag{60}$$

It is a remarkable consequence of the condition $l\le n+1$ that the presence of high partial waves implies a departure of the two-pion distribution amplitude from its asymptotic form. The θ-distribution of the produced pion pair thus contains information about the dependence of the GDAs on z, which as a loop variable is integrated over in the amplitude of the process, cf. Eq. (12).

One-meson distribution amplitudes are real valued functions due to time reversal invariance. This is not true for generalized distribution amplitudes: the two-pion "out" state in the definition (13) of $\Phi^{\pi\pi}$ is transformed into an "in" state under time reversal, and these states are different because hadrons interact with each other. Below the inelastic threshold, however, two-pion "in" and "out" states with definite angular momentum are related in a simple way via the phase shifts of elastic $\pi\pi$-scattering. With the aid of Watson's theorem one then obtains the relation $\tilde B_{nl}^* = \tilde B_{nl}\exp(-2i\delta_l)$ [19]. This fixes the phase of the expansion coefficient $\tilde B_{nl}$ up to its overall sign:

$$\tilde B_{nl} = \eta_{nl}|\tilde B_{nl}|\,\exp(i\delta_l), \qquad \eta_{nl}=\pm 1, \tag{61}$$

where δ_l is the $\pi\pi$ phase shift for the l-th partial wave in the $I=0$ channel.

F. Momentum sum rule

Of particular interest are the moments

$$\int_0^1 dz\,(2z-1)\Phi_q^+(z,\zeta,W^2) = \frac{2}{(P^+)^2}\,\langle\pi^+(p)\pi^-(p')|\,T_q^{++}(0)\,|0\rangle, \tag{62}$$

$$\int_0^1 dz\,\Phi_g(z,\zeta,W^2) = \frac{1}{(P^+)^2}\,\langle\pi^+(p)\pi^-(p')|\,T_g^{++}(0)\,|0\rangle, \tag{63}$$

where $T_q^{\mu\nu}(x)$ and $T_g^{\mu\nu}(x)$ respectively denote the Belinfante improved energy-momentum tensors for quarks of flavor q and for gluons. After summing (62) over all flavors these moments project out the coefficients $B_{10}(W^2)$, $B_{12}(W^2)$ and $B'_{10}(W^2)$, $B'_{12}(W^2)$.

To proceed one decomposes $\langle\pi^+(p)\pi^-(p')|\,T_q^{\mu\nu}(0)\,|0\rangle$ on form factors. Their analytical continuation to zero or negative W^2 leads to the form factors of the matrix elements $\langle\pi^+(p)|\,T_q^{\mu\nu}(0)\,|\pi^+(p')\rangle$ between one-pion states, with $W^2=0$ corresponding to $p=p'$. At that point we get from Eq. (62)

$$B_{12}(0) = \frac{10}{9n_f}\, R_\pi, \tag{64}$$

where R_π is the fraction of light-cone momentum carried by quarks and antiquarks in the pion. No constraint on $B_{10}(0)$ is obtained this way, since the corresponding form factor in the decomposition of $\langle \pi^+(p)|\, T_q^{\mu\nu}(0)\, |\pi^+(p')\rangle$ is multiplied by a tensor that vanishes for $p = p'$. In an analogous fashion one obtains an expression for $B'_{12}(0)$ from the sum rule (63).

We emphasize that both sides of Eq. (64) depend on the renormalization scale μ. Only the total energy-momentum tensor, i.e., the sum $T^{\mu\nu} = \sum_q T_q^{\mu\nu} + T_g^{\mu\nu}$ over quarks and gluons is conserved, so that its matrix elements are renormalization scale independent. The appropriate sum of the moments (62) and (63) leads to a linear combination of B_{12} and B'_{12} where the scale dependent term with $B_{12}^{(+)}$ indeed drops out and only $B_{12}^{(-)}$ is left. The normalization of $\langle \pi^+(p)|\, T^{\mu\nu}(0)\, |\pi^+(p)\rangle$ thus fixes the expansion coefficient

$$B_{12}^{(-)}(0) = \frac{10}{9n_f + 48}, \tag{65}$$

which through the relation (64) gives the asymptotic value

$$R_\pi \overset{\mu\to\infty}{\to} \frac{3n_f}{3n_f + 16}, \tag{66}$$

in agreement with the well-known result from the evolution of singlet parton distributions [25].

IV. A SIMPLE MODEL OF THE GDA

So far no experimental information exists on the two-pion GDA. In the numerical studies to follow we will therefore use a simple ansatz for $\Phi_q^+(z, \zeta, W^2)$, which is based on the general properties we have discussed in the previous section.

We only consider the contributions from u- and d-quarks, i.e., we take $n_f = 2$. As already mentioned we will use the isospin relations (21) and (22), and take the asymptotic form of the z dependence given in Eq. (59). It thus remains to make an ansatz for the coefficients $B_{10}(W^2)$ and $B_{12}(W^2)$, or equivalently for $\tilde{B}_{10}(W^2)$ and $\tilde{B}_{12}(W^2)$ introduced in Eq. (60).

For their phases, given by Eq. (61), we use simple parameterizations of the isosinglet S- and D-wave phase shifts δ_0 and δ_2 obtained in [26]. They are shown in Fig. 6, where for later use the phase shift δ_1 of the P-wave is also displayed. The result (61) only holds below the inelastic threshold in $\pi\pi$ scattering, therefore we restrict all our studies to invariant masses W below 1 GeV. Around that mass, corresponding to the $K\bar{K}$ threshold, the phase shift δ_0 of the S-wave drastically increases. While the analysis of [26] stops at $W = 0.97$ GeV and does not exhibit this abrupt change, the investigations in Ref. [27] find values of order 200° at $W = 1$ GeV. Our parameterization of δ_0 in that region is meant to be indicative rather than a precise description of this quantity. Through interference effects, the rapid variation of a phase shift leads to a characteristic behavior in the W-spectrum of appropriate observables in our process, as we shall see in Sect. VII.

The analyticity properties of the $\tilde{B}_{nl}$ and the phase information from Watson's theorem (61) may be used to obtain the W^2-dependence of $\tilde{B}_{nl}$ via dispersion relations, which has been exploited in [16,19]. Note, however, that while the complex phases are simple for the $\tilde{B}_{nl}$, it is the B_{nl} that have simple analytic properties in the W^2-plane, given their definition through operator matrix elements. The transformation from B_{nl} to $\tilde{B}_{nl}$ introduces extra poles at $W^2 = 0$, cf., e.g., the factors $\beta^2 = (W^2 - 4m_\pi^2)/W^2$ in Eq. (60). Furthermore, the evaluation of the integrals that solve the dispersion relations requires knowledge of the phases at energies above the value of W where $\tilde{B}_{nl}$ is evaluated. This further restricts the range of W where $\tilde{B}_{nl}$ can be obtained using the $\pi\pi$ phase shifts as input.

To keep our model simple we will make a less sophisticated ansatz. We keep the energy dependent phases δ_0 and δ_2 from Watson's theorem (61). To determine $|\tilde{B}_{10}|$, $|\tilde{B}_{12}|$, and the overall signs η_{10}, η_{12} in Eq. (61), we retain only the kinematical factors β^2 in the relation (60) and replace $B_{10}(W^2)$ and $B_{12}(W^2)$ with their values at $W = 0$. Close to $W = 1$ GeV one will not expect this to be a good approximation for the S-wave, given the presence of the $f_0(980)$. Below this there is however no prominent $\pi\pi$ resonance in the $I = 0$ channel, and the phase shifts show a smooth behavior. It seems therefore reasonable to assume that the isosinglet form factors $\tilde{B}_{10}$ and $\tilde{B}_{12}$ do not have a strong energy dependence in that region, certainly not as strong as the electromagnetic pion form factor F_π with its large variations in modulus and phase due to the $\rho(770)$. We do however not claim our simple model to be better than, say, a factor of 2.

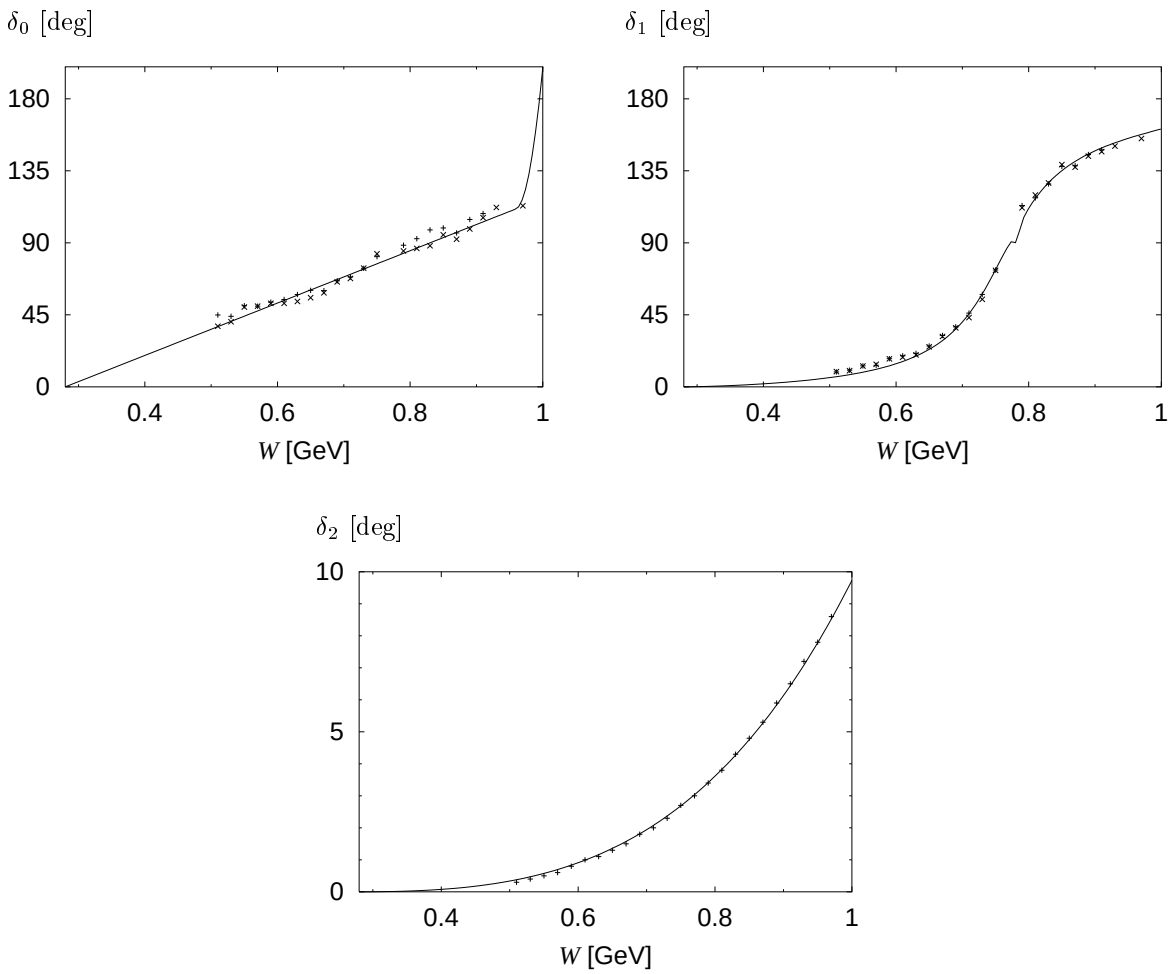

FIG. 6. The phase shifts δ_0 for the S-wave, δ_1 for the P-wave and δ_2 for the D-wave of elastic $\pi\pi$ scattering. δ_0 and δ_2 refer to the $I = 0$ channel. The points are taken from [26], and the curves for δ_0 and δ_2 are simple parameterizations. The curve for δ_1 corresponds to the parameterization $N = 1$ of the pion form factor $F_\pi(W^2)$ in [28].

For the input value of $B_{12}(0)$ we use the constraint (64) with R_π evaluated from the parton distributions in the pion. Taking the LO parameterization of GRS [29] we find R_π ranging from 0.5 to 0.6 at a factorization scale μ^2 between 1 GeV^2 and 20 GeV^2. In our numerical studies we use $R_\pi = 0.5$. Note that this is very far from the asymptotic value (66), which for $n_f = 2, 3, 4$ is $R_\pi = 0.27$, 0.36 and 0.43, respectively. While using the asymptotic form of the z-dependence of the GDA for simplicity (and lack of experimental information) we thus retain a clear non-asymptotic effect in the coefficient $B_{12}(0)$. We also remark that in the GRS LO parameterization the contribution of strange quarks and antiquarks to R_π is at the level of 5% to 10% in a wide range of the factorization scale. This corroborates our restriction to u- and d-quarks in the GDA, although with the caveat that the sea quark distribution in the pion is not constrained from experimental data [29].

For the coefficient $B_{10}(0)$ we make use of the relation

$$B_{10}(0) = -B_{12}(0), \tag{67}$$

which has been obtained in [19] using chiral symmetry in the form of a soft-pion theorem. Notice that our ansatz then has the property that for $\beta \to 1$ the S- and D-wave components of the GDA have equal size and opposite sign, as is easily seen from Eq. (60).

Putting everything together, we will take the following model GDAs in our numerical studies:

$$\Phi_u^+ = \Phi_d^+ = 10z(1-z)(2z-1)\, R_\pi \left[-\frac{3-\beta^2}{2}\, e^{i\delta_0(W^2)} + \beta^2\, e^{i\delta_2(W^2)}\, P_2(\cos\theta) \right] \tag{68}$$

with $R_\pi = 0.5$.

With this we can easily calculate the scattering amplitude for $\gamma^*\gamma \to \pi\pi$ to leading order in α_S. We shall neglect here the radiative corrections to the hard scattering, which have been worked out to one loop in [16]. Taking the asymptotic form (56) of the quark and gluon GDAs, including the asymptotic value (66) of the ratio R_π, they were found to reduce the leading-order amplitude for equal photon helicities by 30% if $\alpha_S = 0.3$, with most of the correction being due to the contribution from Φ_g. Finally, we recall from the end of Sect. III D that we will neglect the contribution of the helicity-two gluon GDA to the photon double helicity-flip amplitude, which is also a one-loop effect.

V. COMPARISON WITH $\gamma^*\gamma \to \pi^0$

Given the close analogy between the production of one and of two pions it is natural to compare the production rates of these two processes. Since our estimations for $\pi\pi$ production are at lowest order in α_S we will compare with the corresponding expression for the one-pion case for consistency, although experimental data and more refined theory analyses are available there. From the leading-order expression (14) we obtain the cross section for the process $e\gamma \to e\pi^0$ as

$$\frac{d\sigma_{e\gamma\to e\pi^0}}{dQ^2} = \frac{\alpha^3}{s_{e\gamma}^2}\, \frac{1}{Q^2(1-\epsilon)}\, 2\pi^2 f_\pi^2 \tag{69}$$

where we have used the asymptotic distribution amplitude $\phi_u^\pi = -\phi_d^\pi = 3\sqrt{2} f_\pi\, z(1-z)$ with $f_\pi \approx 131$ MeV. For a lowest-order approximation, the cross section (69) is in fair agreement with the data [9].

To compare with two-pion production, we integrate the cross section for $e\gamma \to e\,\pi^0\pi^0$ from threshold up to W_{max}. With our model GDA (68) we find

$$\begin{aligned} \frac{d\sigma_{e\gamma\to e\pi^0\pi^0}}{dQ^2} &= \frac{25\,\alpha^3}{72\, s_{e\gamma}^2}\, \frac{1}{Q^2(1-\epsilon)} \int_{4m_\pi^2}^{W_{max}^2} dW^2 \sqrt{1-\frac{4m_\pi^2}{W^2}} \left(|\tilde B_{10}|^2 + \frac{1}{5}|\tilde B_{12}|^2 \right) \\ &= \frac{125\,\alpha^3}{243\, s_{e\gamma}^2}\, \frac{1}{Q^2(1-\epsilon)}\, R_\pi^2 m_\pi^2 \sqrt{1-\frac{4m_\pi^2}{W_{max}^2}} \left(\frac{W_{max}^2}{4m_\pi^2} - \frac{3}{4} - \frac{m_\pi^2}{W_{max}^2} \right). \end{aligned} \tag{70}$$

A consequence of the identical scaling behavior of the two processes is that the ratio of the cross sections (70) and (69) is independent of Q^2 in the Born approximation.

Fig. 7 shows the ratio of the cross sections (70) and (69) as a function of the upper integration limit W_{max}. We see that, even when integrating up to $W = 1$ GeV, the single-pion production comes out as clearly dominant. We remark that the measured production rates [9] for a single η or η' are comparable to that of a π^0. With our isospin

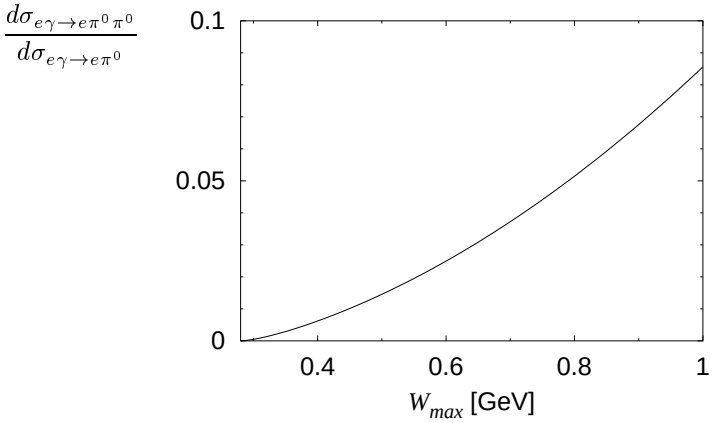

FIG. 7. The ratio of the cross sections (70) and (69) for the production of $\pi^0\pi^0$ and of π^0 in the limit of large Q^2. The cross section for $e\gamma \to e\,\pi^0\pi^0$ is integrated over W from threshold up to W_{max}.

relation (21) the cross section for $\gamma^*\gamma \to \pi^+\pi^-$ is twice that of $\gamma^*\gamma \to \pi^0\pi^0$, the relative factor 1/2 for $\pi^0\pi^0$ being due to the phase space of identical particles. Due to phase space one does not expect the production of more than two pions to be important for W below 1 GeV, except for the decays $\eta \to 3\pi$ and $\eta' \to 5\pi$. The picture thus emerges that with our estimation for $\gamma^*\gamma \to \pi\pi$ the production of hadrons in $\gamma^*\gamma$ collisions up to 1 GeV is dominated by the pseudoscalar channel, in other words by the parity-odd sector as opposed to the parity-even one. This is reminiscent of the special role played by the axial current in low-energy QCD.

At this point we wish to comment on the end-point regions of the integrals over z in the factorized expressions (12) and (14) for two-pion and one-pion production. For $z \to 0$ and $z \to 1$ the hard-scattering kernels are divergent, corresponding to the quark exchanged between the γ and γ^* going on-shell. These poles are canceled by the end-point zeroes of the two-pion and one-pion distribution amplitudes, so that the end-point regions give a finite contribution to the scattering amplitude in both cases. Quantitatively, the quark virtualities in the hard-scattering diagrams are zQ^2 and $(1-z)Q^2$, and it is clear that for a given finite Q^2 there is a region in z where our leading-order expressions should receive important corrections. At small virtualities the strong coupling becomes large, increasing the size of α_S corrections, and when zQ^2 or $(1-z)Q^2$ becomes comparable to the square of typical transverse quark momenta in a pion, then power corrections due to the effect of the transverse momentum of the produced $q\bar{q}$- pair will be important. We recall in this context that various theoretical attempts to evaluate such corrections lead to fair agreement with the data for the γ–π transition form factor [9,30] down to rather low values of Q^2.

For pion pair production both the hard-scattering kernel and the distribution amplitude are zero at $z = 1/2$ due to the constraints from charge conjugation invariance, so that compared to the single-pion case the integral in z is more sensitive to the end-point regions. We thus expect that for intermediate values of Q^2 corrections to the lowest-order results will be more important in $\gamma^*\gamma \to \pi\pi$ than they are in $\gamma^*\gamma \to \pi^0$. The experimental comparison of the Q^2-dependence of these two processes will therefore be interesting and may help us to better understand the origin of these corrections, which are a subject of considerable importance in the physics of exclusive processes.

Taking the asymptotic z-dependence of the distribution amplitudes as an example, we can explicitly see how important the end-point contributions are in the leading-order expressions (12) and (14). For single pion production the integrand in Eq. (14) is a constant then, so that 50% of the z-integral comes from the regions where z or $1-z$ is smaller than 0.25. For two-pion production the integrand is proportional to $(2z-1)^2$, and 50% of the integrand comes from the regions with z or $1-z$ smaller than $(1-2^{-1/3})/2 \approx 0.1$. Given these numbers, one can expect that corrections to our leading-order calculation will not be negligible for Q^2 around 4 GeV^2, which is the lowest value considered in our numerical estimates in Sect. VIII.

VI. RELATIONS WITH THE PHOTON STRUCTURE FUNCTION

The exclusive process we consider here contributes of course to the inclusive reaction $\gamma^*\gamma \to X$. As we mentioned in the previous section, the inclusive process is built up from a limited number of exclusive channels in the mass region of W below 1 GeV. Let us examine the connection between our discussion of one- and two-pion production with the familiar description of inclusive $\gamma^*\gamma$ scattering in the kinematical limit we are taking here.

The unpolarized cross section for inclusive deep inelastic scattering on a photon, $e\gamma \to eX$, can be parameterized by two photon structure functions F_T and F_L as

$$\frac{d\sigma_{e\gamma\to eX}}{dQ^2\,dW^2} = \frac{2\pi\alpha^2}{s_{e\gamma}^2}\,\frac{1}{xQ^2(1-\epsilon)}\,\left(2xF_T(x,Q^2)+\epsilon F_L(x,Q^2)\right), \tag{71}$$

where F_T and F_L respectively give the contribution from transverse and longitudinal polarization of the exchanged γ^*. The transverse structure function F_T is often traded for $F_2 = 2xF_T + F_L$.

At the level of partons inclusive hadron production is described by $\gamma^*\gamma \to q\bar{q}$ to leading order in α_S, which gives the well-known expressions [2]

$$\begin{aligned} F_T^{q\bar{q}} &= \frac{3\alpha}{2\pi}\sum_q e_q^4\left\{\ln\frac{1+\beta_q}{1-\beta_q}\left[x^2+(1-x)^2+4x(1-x)\frac{m_q^2}{Q^2}-8x^2\frac{m_q^4}{Q^4}\right]-\beta_q\left[(1-2x)^2+4x(1-x)\frac{m_q^2}{Q^2}\right]\right\}, \\ F_L^{q\bar{q}} &= \frac{12\alpha}{\pi}\sum_q e_q^4\,x^2(1-x)\left[\beta_q-\frac{2m_q^2}{W^2}\ln\frac{1+\beta_q}{1-\beta_q}\right], \end{aligned} \tag{72}$$

where $\beta_q = (1-4m_q^2/W^2)^{1/2}$. Note that m_q is to be understood here as a cutoff parameter, which regulates the collinear divergence in the box diagram with massless quarks.

The limit of large Q^2 at fixed small W^2 we are taking here implies $x \to 1$ and is different from the Bjorken limit, where W^2 is scaled up with Q^2 so that x remains constant. Neglecting terms of order $1-x \sim W^2/Q^2$ and m_q^2/Q^2 the expressions (72) become

$$F_T^{q\bar{q}} = \frac{3\alpha}{2\pi}\sum_q e_q^4\left\{\ln\frac{1+\beta_q}{1-\beta_q}-\beta_q\right\}, \qquad F_L^{q\bar{q}} = O\left(\frac{W^2}{Q^2}\right). \tag{73}$$

We observe that in our limit the leading-order expression for F_T becomes independent of Q^2, i.e., it has the same scaling behavior as the exclusive channels $\gamma^*\gamma \to \pi$ and $\gamma^*\gamma \to \pi\pi$. This is to be contrasted with the Bjorken limit, where $\ln[(1+\beta_q)/(1-\beta_q)] \sim \ln[Q^2/m_q^2] + \ln[(1-x)/x]$ gives rise to the well-known logarithmic scaling violation of F_T at zeroth order in α_S.

Just as in the case of $\gamma^*\gamma \to \pi\pi$, the contribution F_L from longitudinal photons is power suppressed in our limit. Let us add that in the Bjorken limit the hadronic part of F_T, often parameterized using vector meson dominance, is only suppressed by a factor $\ln Q^2$ with respect to the pointlike part (72), but does not survive our limiting procedure here: since hadronic structure functions typically decrease like a power of $1-x$ for $x \to 1$, it becomes a correction in W^2/Q^2.

The contribution of our process to the structure functions is, with our ansatz (68) for Φ_q^+,

$$F_T^{\pi^+\pi^-+\pi^0\pi^0} = \frac{25\,\alpha}{96\,\pi}\,\beta\left(|\tilde{B}_{10}|^2+\frac{1}{5}|\tilde{B}_{12}|^2\right) = \frac{625\,\alpha}{3456\,\pi}\,R_\pi^2\,\beta\left(1-\frac{2}{3}\beta^2+\frac{1}{5}\beta^4\right). \tag{74}$$

As a function of W this quickly rises from the threshold at $2m_\pi$, levels off for W around 400 to 500 MeV, and then remains flat with a value $F_T^{\pi^+\pi^-+\pi^0\pi^0}/\alpha \approx 0.0077$. Let us compare this with the result (73) of the $q\bar{q}$ calculation for u- and d-quarks (including strange quarks would only lead to a minute change due to the charge factor e_q^4). With the quark masses $m_u = m_d = 290$ MeV from the parameterization of the photon structure function by Gordon and Storrow [31] we get a value of $F_T^{q\bar{q}}/\alpha \approx 0.15$ at $W = 1$ GeV, much larger than the one we obtain for pion pairs.

It is worth remembering that $\gamma^*\gamma \to q\bar{q}$ also is the hard-scattering subprocess in our factorized expression for $\gamma^*\gamma \to \pi\pi$. As we discussed at the end of the previous section, the collinear divergence of this process shows up as singularities at the end-points of the z-integration in Eq. (12) and is canceled by the end-point zeroes of the GDA, i.e., by the hadronization process. In the calculation of open $q\bar{q}$ production no such cancellation takes place and the divergence of the diagram has to be regulated. This reflects the fact that even in the limit $Q^2 \to \infty$ inclusive hadron production from $\gamma^*\gamma$ cannot be calculated in perturbation theory alone (unlike for instance inclusive hadron production from a single timelike photon) and that the separation of F_T into a perturbative pointlike and a non-perturbative hadronic part is not unambiguous. While more sophisticated procedures have been elaborated in the literature, we consider it sufficient for our purpose to use the quark mass regulator in Eq. (73). One might also take massless quarks and a lower cutoff $\kappa_\perp$ on the transverse quark momentum, obtaining the same result (73) with m_q replaced by $\kappa_\perp$ in the expression of β_q. While keeping us away from the region where perturbation theory breaks down, such phenomenological regulators become of course inadequate as one approaches the "threshold" where $\beta_q = 0$.

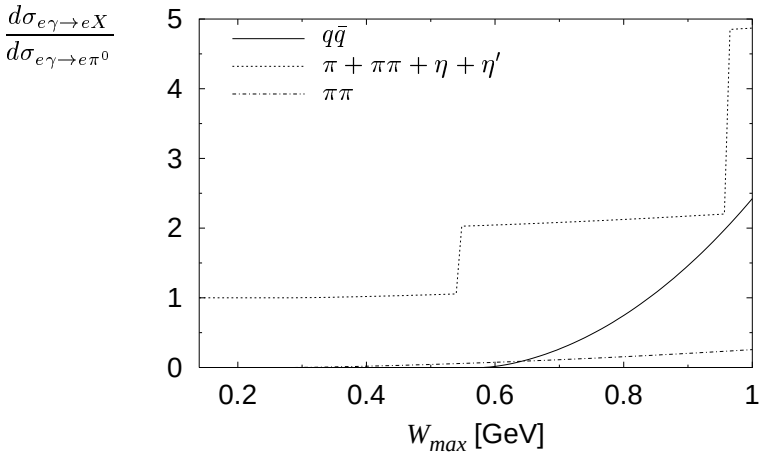

FIG. 8. The cross section $d\sigma_{e\gamma\to eX}/dQ^2$ for inclusive hadron production, integrated over W from threshold up to W_{max}, and normalized to the cross section (69) for one-pion production. The solid curve is the result of the $q\bar{q}$-calculation (73), and the dotted curve is the sum over the individual contributions from π^0, $\pi^+\pi^-$, $\pi^0\pi^0$, η and η'. The dash-dotted curve shows the contribution from pion pairs $\pi^+\pi^-$ and $\pi^0\pi^0$ alone.

For our numbers this is at $W = 580$ MeV. One should bear this in mind when using the expression (73) for masses W around 1 GeV.

On the other hand we saw in Sect. V that with our estimate of two-pion production the hadronic mass spectrum below 1 GeV is dominated by the single-meson states π^0, η, η'. It is clear that in such a region the parton-level result can only hold in the sense of parton-hadron duality, averaged over a sufficiently large interval in W. We therefore integrate the cross section for $e\gamma \to eX$ over W from threshold to W_{max}. In Fig. 8 we compare the parton level result, obtained from Eq. (73) with $m_u = m_d = 290$ MeV, with the sum of the individual contributions from two pions (74), one pion (69), and the η and η'. For the latter we take again the asymptotic distribution amplitudes, and replace $f_\pi = 131$ MeV in Eq. (69) with 129 MeV for the η and 213 MeV for the η', taken from the analysis of [30]. Given the caveats discussed above, we find the agreement at larger values of W remarkably good.

VII. PHENOMENOLOGY

We will now discuss the phenomenology of our process in $e\gamma$ and in e^+e^- collisions. The production of neutral and charged pion pairs is rather different in this respect, since $\pi^0\pi^0$ is only produced by the $\gamma^*\gamma$ subprocess we have discussed so far, whereas for $\pi^+\pi^-$ production this process interferes with bremsstrahlung, i.e., the production of the pion pair from a timelike photon radiated off the beam lepton. We start with the simpler case of neutral pions, and then discuss charged pairs. In the following we will restrict ourselves to unpolarized photon and lepton beams. A brief discussion of beam polarization will be given in Appendix B.

A. Helicity amplitudes

The building blocks of our investigation are the helicity amplitudes for $\gamma^*\gamma \to \pi\pi$, which describe the dynamics of this process in a model independent way. They are obtained from the hadronic tensor $T^{\mu\nu}$ by multiplying the reduced amplitudes

$$A_{ij}(Q^2, W^2, \theta) = \epsilon_i^\mu \, T_{\mu\nu} \epsilon'^\nu_j, \qquad i = +, 0, -, \qquad j = +, - \tag{75}$$

with the squared elementary charge e^2. In the $\gamma^*\gamma$ c.m. our photon polarization vectors read

$$\epsilon_0 = \frac{1}{Q}\,(|\mathbf{q}\,|, 0, 0, q^0), \qquad \epsilon_\pm = \frac{1}{\sqrt{2}}\,(0, \mp 1, -i, 0) \tag{76}$$

for the virtual and

$$\epsilon'_{\pm} = \frac{1}{\sqrt{2}}\,(0, \mp 1, +i, 0) \tag{77}$$

for the real photon, where we have used the coordinate system described in Sect. II A. By parity invariance, there are only three independent helicity amplitudes, which we choose to be A_{++}, A_{-+} and A_{0+}.

Each of these three amplitudes plays a distinctive dynamical role in the kinematical region $Q^2 \gg W^2, \Lambda^2$. It is A_{++} that receives the leading twist contribution we have discussed in detail, and which in the scaling regime gives access to the generalized quark distribution amplitudes $\Phi_q^{\pi\,\pi}$,

$$A_{++} = \sum_q \frac{e_q^2}{2} \int_0^1 dz\, \frac{2z-1}{z(1-z)}\, \Phi_q^{\pi\,\pi}(z, \zeta, W^2) \tag{78}$$

to zeroth order in α_S. The amplitude A_{-+} has a leading-twist part at order α_S, due to the helicity-two gluon GDA. We briefly discussed this at the end of Sect. III D; for more detail we refer to [16]. Finally, the contribution A_{0+} from a longitudinal γ^* is nonleading twist. The predicted power behavior in Q^2 at fixed W^2 and ζ is therefore that A_{++} becomes independent of Q^2, whereas A_{0+} decreases at least like $1/Q$. The amplitude A_{-+} should become Q^2-independent. If the helicity-two gluon GDA is however not sufficiently large, A_{-+} may be dominated by higher-twist contributions at accessible values of Q^2 and should decrease like a power of $1/Q$ in the corresponding Q^2-range. Of course all these predictions are to be understood as up to corrections in $\log Q^2$. At sufficiently large Q^2, the longitudinal amplitude A_{0+} is thus predicted to be small compared with A_{++}. One can also expect that A_{-+} will be smaller than A_{++}, since its leading-twist part is suppressed by α_S.

To discuss the different partial waves in which the pion pair can be produced, we expand each of the amplitudes A_{++}, A_{0+}, A_{-+} as

$$A_{ij} = \sum_{\substack{l=j-i \\ \text{even}}}^{\infty} A_{ijl}(Q^2, W^2)\, P_l^{j-i}(\cos\theta), \qquad i = +, 0, -, \qquad j = +, \tag{79}$$

where P_l^m denotes the associated Legendre polynomial corresponding to the value of J_z of the $\pi\pi$ system in its c.m.

B. The $\gamma^*\gamma$ subprocess and $\pi^0\pi^0$ production

The differential $e\gamma$ cross section for neutral pion pair production reads

$$\begin{aligned}\left.\frac{d\sigma_{e\gamma\to e\,\pi\,\pi}}{dQ^2\,dW^2\,d(\cos\theta)\,d\varphi}\right|_G = \frac{\alpha^3}{16\pi}\,\frac{\beta}{s_{e\gamma}^2}\,\frac{1}{Q^2(1-\epsilon)}\,\Big(\,&|A_{++}|^2 + |A_{-+}|^2 + 2\epsilon\,|A_{0+}|^2 \\ &- \cos\varphi\,\mathrm{Re}\left\{A_{++}^* A_{0+} - A_{-+}^* A_{0+}\right\} 2\sqrt{\epsilon(1+\epsilon)} \\ &- \cos 2\varphi\,\mathrm{Re}\left\{A_{++}^* A_{-+}\right\} 2\epsilon\,\Big),\end{aligned} \tag{80}$$

where the subscript G indicates that the pions are produced in a $\gamma^*\gamma$ subprocess. For $\pi^0\pi^0$ production the phase space in Eq. (80) is understood as restricted to $\cos\theta \in (0,1)$, $\varphi \in (0, 2\pi)$ because there are two identical particles in the final state. We notice the close similarity of the expression (80) with the cross section of the crossed channel process of virtual Compton scattering, and much of what we discuss in the following has its counterpart there [14].

To obtain the e^+e^- cross section we use the equivalent photon approximation [2],

$$\frac{d\sigma_{ee\to ee\,\pi\,\pi}}{dQ^2\,dW^2\,d(\cos\theta)\,d\varphi\,dx_2} = \frac{\alpha}{\pi}\,\frac{1}{x_2}\left(\frac{1+(1-x_2)^2}{2}\ln\left[\frac{Q'^2_{max}(x_2)}{Q'^2_{min}(x_2)}\right] - (1-x_2)\right)\,\frac{d\sigma_{e\gamma\to e\,\pi\,\pi}}{dQ^2\,dW^2\,d(\cos\theta)\,d\varphi}, \tag{81}$$

where Q'^2_{min} and Q'^2_{max} are the minimal and maximal virtuality of the photon q', respectively. We have a lower kinematical limit $Q'^2_{min} = x_2^2\, m_e^2/(1-x_2)$ determined by the electron mass m_e, whereas Q'^2_{max} depends on experimental cuts and will be discussed in more detail in Sect. VIII A. We remark that for a given ee collider energy the variables x_2 and y are not independent at fixed Q^2 and W^2, since

$$y x_2 = \frac{Q^2 + W^2}{s_{ee}}, \tag{82}$$

and that in Eq. (81) one can easily trade dx_2 for dy.

Since the helicity amplitudes A_{ij} are independent of φ they can be partially disentangled from the φ-dependence of the cross section, which is completely explicit in Eq. (80). In particular, the relative size and the Q^2-behavior of the φ-independent term and of the terms with $\cos\varphi$ and $\cos 2\varphi$ allow detailed tests of the scaling predictions. This provides indicators on how close one is to the asymptotic regime at finite values of Q^2. The φ-independent term in the large parentheses of Eq. (80) receives contributions from leading-twist amplitudes and should thus display scaling behavior. The coefficient of $\cos\varphi$ is the interference of leading-twist and non-leading twist amplitudes and should be suppressed by at least one power of $1/Q$. Finally, the $\cos 2\varphi$ term should scale or be power suppressed depending on the size of the helicity-two gluon GDA.

Apart from standard fitting techniques a way to separate terms with different angular dependence is the use of weighted cross sections. Weighting each event with a function $w(\varphi,\theta)$ we define

$$S_{e\gamma}(w) = \int dQ^2 dW^2 d\Omega \, \frac{d\sigma_{e\gamma}}{dQ^2 dW^2 d\Omega} \, w(\varphi,\theta), \tag{83}$$

where $d\Omega = d(\cos\theta)\, d\varphi$. Notice that since it is not normalized, $S_{e\gamma}(w)$ is not just the average value of the function $w(\varphi,\theta)$, and includes information about the size of the cross section itself. Interpreting $S_{e\gamma}(w)$ as a statistical variable one can calculate its standard deviation and finds for its relative statistical error (cf., e.g., [32])

$$\delta(w) = \frac{1}{\sqrt{N}} \, \frac{\sqrt{\int dQ^2 dW^2 d\Omega \, \frac{d\sigma_{e\gamma}}{dQ^2 dW^2 d\Omega} \, w^2(\varphi,\theta)} \, \sqrt{\int dQ^2 dW^2 d\Omega \, \frac{d\sigma_{e\gamma}}{dQ^2 dW^2 d\Omega}}}{\left| \int dQ^2 dW^2 d\Omega \, \frac{d\sigma_{e\gamma}}{dQ^2 dW^2 d\Omega} \, w(\varphi,\theta) \right|}, \tag{84}$$

where

$$N = \mathcal{L} \int dQ^2 dW^2 d\Omega \, \frac{d\sigma_{e\gamma}}{dQ^2 dW^2 d\Omega} \tag{85}$$

is the expected number of events for a given integrated luminosity $\mathcal{L}$. Eq. (84) generalizes the well-known result that the relative statistical error of the cross section, i.e., of $S_{e\gamma}(1)$, is $1/\sqrt{N}$. We emphasize that the method of weighted cross sections is very flexible, and that the choice of weights $w(\varphi,\theta)$ can for instance be adapted to experimental conditions such as limited angular acceptance or cuts. One can of course take weighting functions that depend on other variables than only θ and φ. In the following we will also use weighted differential cross sections, where only some of the kinematical variables have been integrated out while others are held fixed. In a data analysis, one may thus use the weighting technique for some variables and fitting for others.

The weighting technique is convenient to project out different terms in the cross section. As an immediate example we note that the terms constant in φ, with $\cos\varphi$, and with $\cos 2\varphi$ in the $e\gamma$ cross section are obtained from

$$\frac{dS_{e\gamma}(\cos m\varphi)}{dQ^2\, dW^2\, d(\cos\theta)} \tag{86}$$

with $m = 0$, 1 and 2, respectively. If the moments with $m = 1$ and 2 are measured to be small compared with the moment $m = 0$, this can be because any two of the amplitudes A_{++}, A_{0+}, A_{-+} are much smaller than the third, or it may be due to their relative phases. From the theoretical considerations in Sect. VII A the most natural hypothesis in this case is however that A_{0+} and A_{-+} are small compared with A_{++}.

While the φ-dependence of the cross section (80) gives access to the various helicity combinations of the real and virtual photon, its dependence on θ contains information on the angular momentum states in which the pion pair is produced. A priori there can be arbitrarily high partial waves, but to analyze the θ-distribution in practice one will assume that at a given W only a finite number of them is important, if only for reasons of phase space. It is easy to see from Eqs. (79) and (80) that for a superposition of partial waves $l = 0,\, 2,\, \ldots L$ the moment of $\cos m\varphi$ in (86) is a linear combination of polynomials $P_{2l}^m(\cos\theta)$ with highest degree $2L$. Weighting the cross section with $\cos(m\varphi)\, P_{2L+2}^m(\cos\theta)$ and integrating over φ and θ then gives a zero result. Using these weights thus provides one way to estimate from experimental data how many partial waves are relevant. Let us recall the physical relevance of this information: in the scaling regime the highest partial wave relevant in A_{++} provides a constraint on how far the two-pion distribution amplitude is from its asymptotic form, as we discussed in Sect. III E.

Let us assume that only partial waves with $l \leq L$ effectively contribute in the cross section (80). The θ-dependence of the moments in (86) is then determined by $L+1$ coefficients for $m = 0$, L coefficients for $m = 1$ and L coefficients

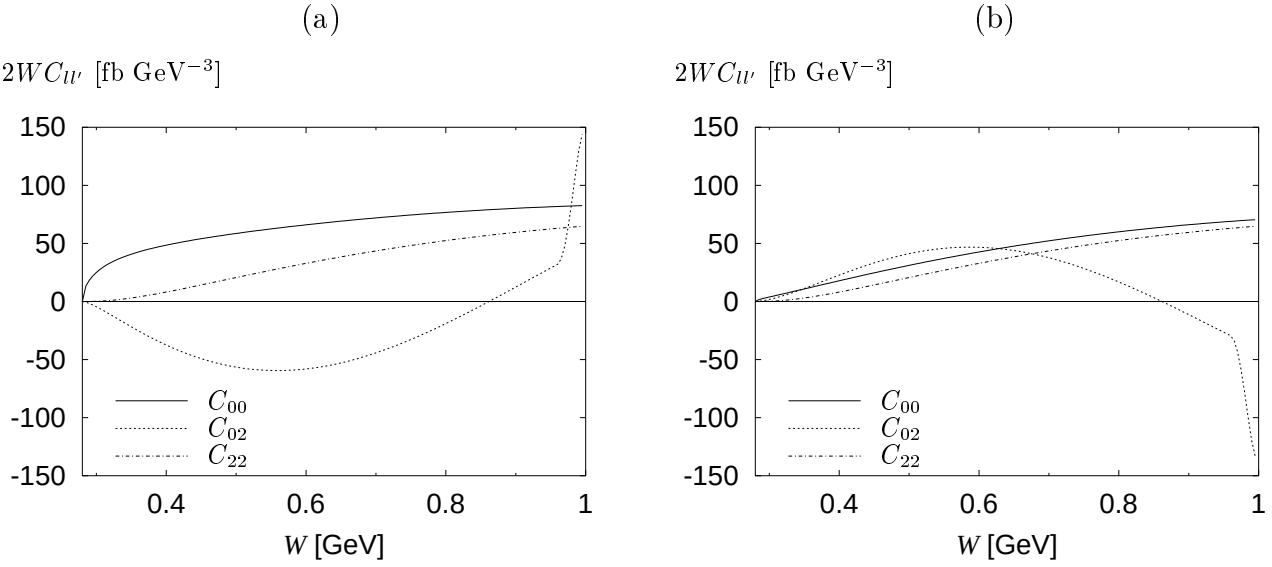

FIG. 9. (a) The coefficients $C_{ll'}$ in the differential cross section (87), evaluated with our model GDA (68). They are plotted against W instead of W^2 and therefore have been multiplied with a Jacobian $2W$. The values of the remaining kinematical variables are $s_{e\gamma} = 50$ GeV^2 and $Q^2 = 5$ GeV^2. (b) The same with the alternative ansatz for the GDA described in the text.

for $m = 2$, corresponding to the number of polynomials $P_{2l}^m(\cos\theta)$ with $l \leq L$. On the other hand, there are $3L/2 + 1$ complex amplitudes A_{ijl} with $l \leq L$ in the expansion (79), so that there are $3L + 2$ real quantities one would like to determine. A global phase is however unobservable in the cross section (80), and one may for instance refer all phases to the phase of A_{++0}. The $3L + 1$ coefficients one can extract from the dependence of the cross section on φ and θ thus allow one to reconstruct the $|A_{ijl}|$ and their relative phases. Since the relation between the angular coefficients and the amplitudes is quadratic, there will however be multiple solutions in general. More information can be obtained with polarized beams, which we briefly discuss in Appendix B.

The situation is simplest if the θ-dependence of the cross section is compatible with the $\pi^0\pi^0$ system being produced only in an S- and a D-wave, and if in addition the φ-dependence is flat. Assuming that A_{0+} and A_{-+} are negligible compared to A_{++}, one can then decompose

$$\frac{d\sigma_{e\gamma\to e\,\pi^0\pi^0}}{dQ^2\,dW^2\,d(\cos\theta)} = C_{00} + C_{02}\,P_2(\cos\theta) + C_{22}\,[P_2(\cos\theta)]^2 \tag{87}$$

and project out the coefficients, using that $C_{ll'} = dS_{e\gamma}(w_{ll'})/(dQ^2\,dW^2)$ with weights

$$\begin{aligned} w_{00} &= -\frac{5}{16}\,(1 - 42\cos^2\theta + 49\cos^4\theta), \\ w_{02} &= -\frac{35}{8}\,(1 - 6\cos^2\theta + 5\cos^4\theta), \\ w_{22} &= \frac{35}{16}\,(3 - 30\cos^2\theta + 35\cos^4\theta). \end{aligned} \tag{88}$$

From these coefficients one can readily extract the amplitudes $|A_{++0}|$, $|A_{++2}|$, and the cosine of their relative phase.

In Fig. 9 (a) we show the coefficients C_{00}, C_{02} and C_{22} obtained with our model GDA (68). The interference term between the S- and D-waves contains a factor $\cos(\delta_0 - \delta_2)$ and thus is sensitive to the phase shifts. Characteristic features in the W-dependence of C_{02} are the point where $\delta_0 - \delta_2 = 90^\circ$, and the sudden change just below $W = 1$ GeV due to the behavior of the S-wave. To explore the dependence of these observables on our input GDA we have made an ad hoc modification, changing the sign in the prediction (67) from chiral dynamics and taking instead $B_{10}(0) = B_{12}(0)$ with $B_{12}(0)$ fixed by the constraint (64) as before. Notice that this flips the overall sign η_{10} of the S-wave in our model. The result is shown in Fig. 9 (b) and illustrates the sensitivity, especially of the S-D interference, to the detailed dynamics of the $\gamma^*\gamma$ process.

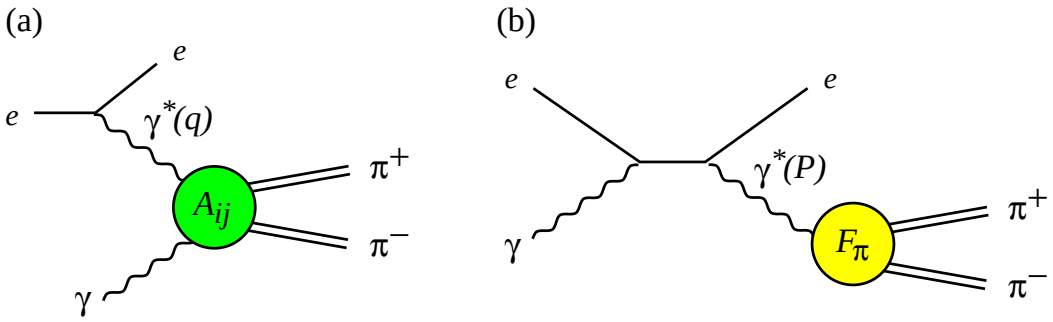

FIG. 10. The two subprocesses contributing to the reaction $e\gamma \to e\,\pi^+\pi^-$: (a) $\gamma^*\gamma$ scattering and (b) bremsstrahlung. There is a second bremsstrahlung diagram, where the photon vertices are interchanged on the lepton line.

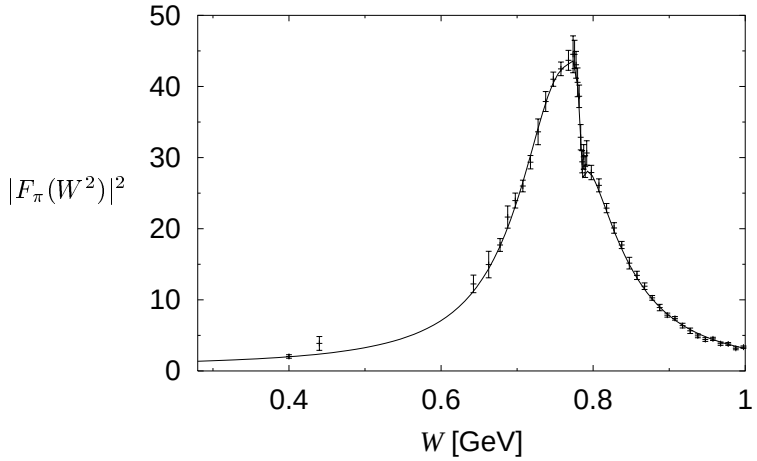

FIG. 11. The square of the electromagnetic pion form factor in the timelike region. The data points are from [33] and the curve is the parameterization $N = 1$ of [28].

C. Production of $\pi^+\pi^-$ and interference with bremsstrahlung

For the production of $\pi^+\pi^-$ pairs in $e\gamma$ collisions, the $\gamma^*\gamma$ reaction we want to study competes with bremsstrahlung, where the pion pair originates from a virtual photon radiated off the lepton [2], cf. Fig. 10. This process produces the pion pair in the C-odd channel and hence does not contribute for $\pi^0\pi^0$. Its amplitude can be fully computed for values of W where the timelike electromagnetic pion form factor $F_\pi(W^2)$ is known. The modulus of F_π has been well measured in $e^+e^- \to \pi^+\pi^-$. By Watson's theorem its phase is equal to the P-wave phase shift δ_1, provided that W is in the range where $\pi\pi$ scattering is elastic. This is rather well satisfied for W up to 1 GeV. In our numerical studies we use for F_π the parameterization $N = 1$ of [28], which is in good agreement with the data for $|F_\pi|^2$ shown in Fig. 11. It also gives a fair description of the phase of F_π in the W-range where we use it, as we see from the comparison with the phase shift δ_1 in Fig. 6.

The contribution of the $\gamma^*\gamma$ subprocess to the cross section of $e\gamma \to e\,\pi^+\pi^-$ has the same form (80) as for $e\gamma \to e\,\pi^0\pi^0$. We recall that with the isospin relation (21) the leading-twist helicity amplitude A_{++} in (78) is the same for neutral and for charged pion pairs. The bremsstrahlung contribution reads

$$\begin{aligned}\left.\frac{d\sigma_{e\gamma\to e\,\pi\pi}}{dQ^2\,dW^2\,d(\cos\theta)\,d\varphi}\right|_B = \frac{\alpha^3}{16\pi}\,\frac{\beta}{s_{e\gamma}^2}\,\frac{2\beta^2}{W^2\,\epsilon}\,|F_\pi(W^2)|^2\,\Big(\,&[1-2x(1-x)]\sin^2\theta + 4x(1-x)\,\epsilon\cos^2\theta \\ &+ \cos\varphi\,\sqrt{2x(1-x)}\,(2x-1)\sqrt{\epsilon(1+\epsilon)}\,2\sin\theta\cos\theta \\ &- \cos 2\varphi\,x(1-x)\,2\epsilon\sin^2\theta\,\Big).\end{aligned} \tag{89}$$

Finally, the interference term of the two subprocesses can be written as[2]

$$\left.\frac{d\sigma_{e\gamma\to e\,\pi\pi}}{dQ^2\,dW^2\,d(\cos\theta)\,d\varphi}\right|_I = -2e_l\,\frac{\alpha^3}{16\pi}\,\frac{\beta}{s_{e\gamma}^2}\,\frac{\sqrt{2}\beta}{\sqrt{W^2Q^2\epsilon(1-\epsilon)}}\Big(C_0 + C_1\,\cos\varphi + C_2\cos 2\varphi + C_3\cos 3\varphi\Big) \tag{90}$$

with $e_l = 1$ for positrons and -1 for electrons, and coefficients

$$\begin{aligned}
C_0 &= \mathrm{Re}\Big\{F_\pi^* A_{++}\Big\}\,\sqrt{2x(1-x)}\sqrt{\epsilon(1+\epsilon)}\cos\theta \\
&\quad +\mathrm{Re}\Big\{F_\pi^* A_{0+}\Big\}\,(1-x)\sqrt{\epsilon(1+\epsilon)}\sin\theta, \\
C_1 &= \mathrm{Re}\Big\{F_\pi^* A_{++}\Big\}\,[1-(1-x)(1+\epsilon)]\sin\theta \\
&\quad -\mathrm{Re}\Big\{F_\pi^* A_{0+}\Big\}\,\sqrt{2x(1-x)}\,2\epsilon\cos\theta \\
&\quad +\mathrm{Re}\Big\{F_\pi^* A_{-+}\Big\}\,(1-x)\sin\theta, \\
C_2 &= -\mathrm{Re}\Big\{F_\pi^* A_{0+}\Big\}\,x\sqrt{\epsilon(1+\epsilon)}\sin\theta \\
&\quad -\mathrm{Re}\Big\{F_\pi^* A_{-+}\Big\}\,\sqrt{2x(1-x)}\sqrt{\epsilon(1+\epsilon)}\cos\theta, \\
C_3 &= -\mathrm{Re}\Big\{F_\pi^* A_{-+}\Big\}\,x\epsilon\sin\theta.
\end{aligned} \tag{91}$$

Remember that in our kinematical limit $1-x \sim W^2/Q^2$ is small. The structure of the bremsstrahlung contribution (89) then becomes rather simple, since at $Q^2 \gg W^2$ the terms in large parentheses reduce to $\sin^2\theta$. With the scaling predictions for the $\gamma^*\gamma$ amplitudes discussed in Sect. VII A we also obtain the Q^2-behavior for each of the coefficients C_n in the interference term (90).

The relative dependence on Q^2, W^2 and on ϵ of the three contributions to the cross section is controlled by the prefactors

$$\frac{1}{Q^2(1-\epsilon)}, \qquad \frac{2\beta^2}{W^2\,\epsilon}, \qquad \frac{\sqrt{2}\beta}{\sqrt{W^2Q^2\epsilon(1-\epsilon)}} \tag{92}$$

for $\gamma^*\gamma$, bremsstrahlung and their interference, respectively, and by the pion form factor $F_\pi(W^2)$, which appears linearly in the interference and squared in the pure bremsstrahlung term. The factors Q^2 and W^2 in (92) can be traced back to the propagator of the virtual photon in each subprocess, and the extra factor of β in the bremsstrahlung amplitude reflects the fact that the pion pair is produced in the P-wave there.

From the factors (92) it follows that the $\gamma^*\gamma$ contribution decreases faster with Q^2 than bremsstrahlung. On the other hand the $\gamma^*\gamma$ process is enhanced at large ϵ, whereas bremsstrahlung profits from small ϵ. To study the amplitudes A_{ij} either in the $\gamma^*\gamma$ contribution or in the interference term, one will therefore go to larger values of ϵ, corresponding to small or intermediate values of y (notice that $\epsilon = 0.8$ corresponds to $y = 0.5$). The behavior in Q^2 and y of the different contributions to the ee cross section can be seen in Figs. 12 and 13, respectively, which have again been obtained with our model GDA (68). Notice that apart from the factors (92) just discussed, there is a global dependence on y and Q^2 through the factor $1/s_{e\gamma}^2$ in the $e\gamma$ cross section and through the variable x_2 in the real photon flux, cf. Eqs. (9) and (82).

A very strong effect on the relative weight of the different contributions comes from the pion form factor $F_\pi(W^2)$. As one can anticipate from Fig. 11 it leads to a considerable enhancement of the bremsstrahlung term in a broad W interval around the ρ mass, thereby also enhancing the interference. The W^2-dependence of the different terms, obtained with of our ansatz (68) for the GDA, are shown in Fig. 14. As we discussed in Sect. IV this ansatz most likely oversimplifies the W^2-dependence of the coefficients B_{10} and B_{12} in Φ_q^+, but the corresponding error in estimating the W^2-behavior of A_{++} should not change the qualitative picture of Fig. 14.

In the limit of large Q^2 the different contributions to the cross section have distinctive dependences on φ. The $\gamma^*\gamma$ contribution is predicted to be constant in φ with a $\cos 2\varphi$ modulation due to the product $A_{++}^* A_{-+}$. The

[2] A C program containing the expressions (80), (89), (90), (91), as well as the amplitude A_{++} calculated with our model GDA (68), can be obtained from the authors.

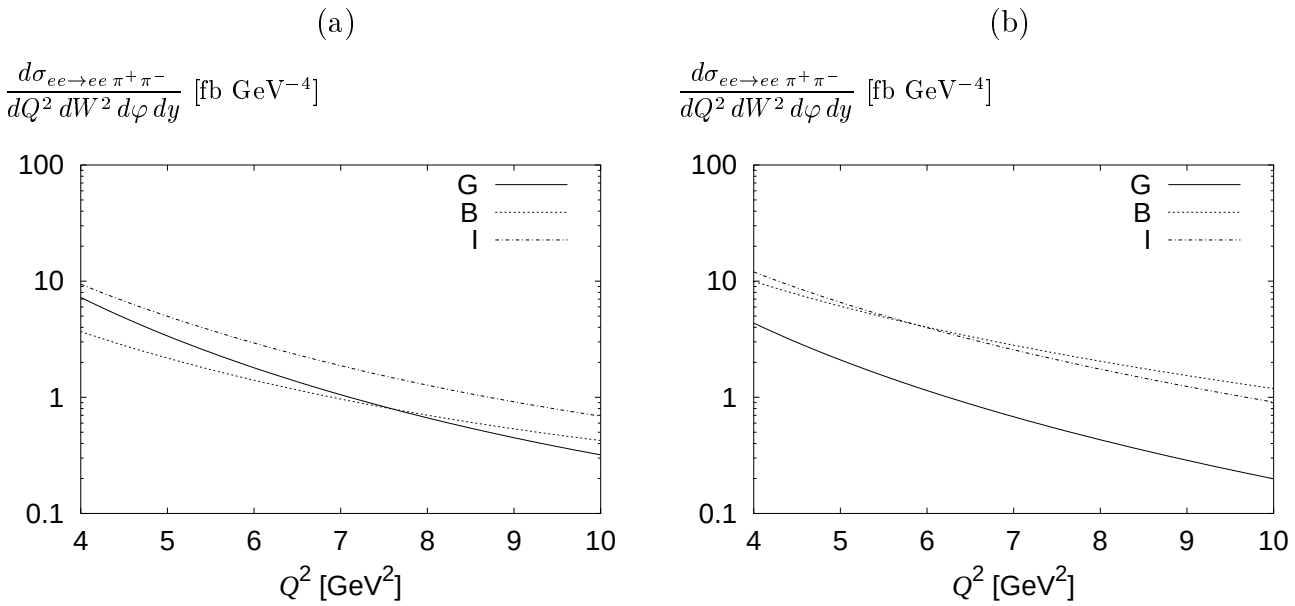

FIG. 12. (a) The contributions to the differential ee cross section from $\gamma^*\gamma$, bremsstrahlung and their interference. Kinematical variables are $W = 400$ MeV, $\varphi = 0$, $y = 0.1$, $E_1 = 3.1$ GeV, $E_2 = 9$ GeV. For the real photon flux in (81) we take $\alpha_{2L}^{max} = 300$ mrad and $l'^{max}_{\perp L} = 100$ MeV as explained in Sect. VIII A. The sign of the interference term corresponds to an $e^+\gamma$ subprocess. (b) The same as (a), but with $y = 0.2$.

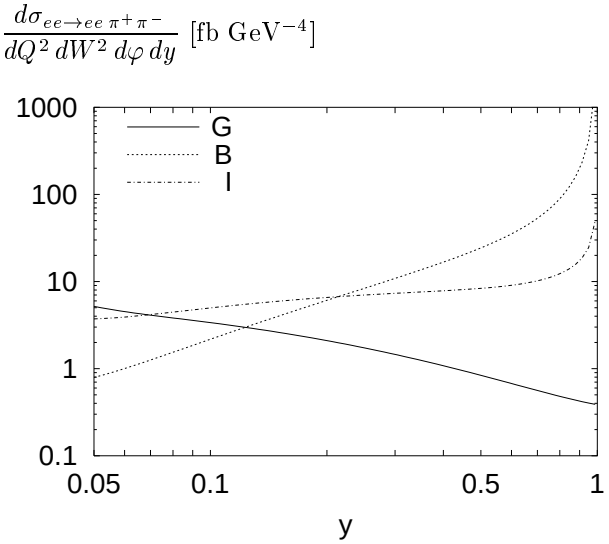

FIG. 13. The same as Fig. 12, but as a function of y at $Q^2 = 5$ GeV^2.

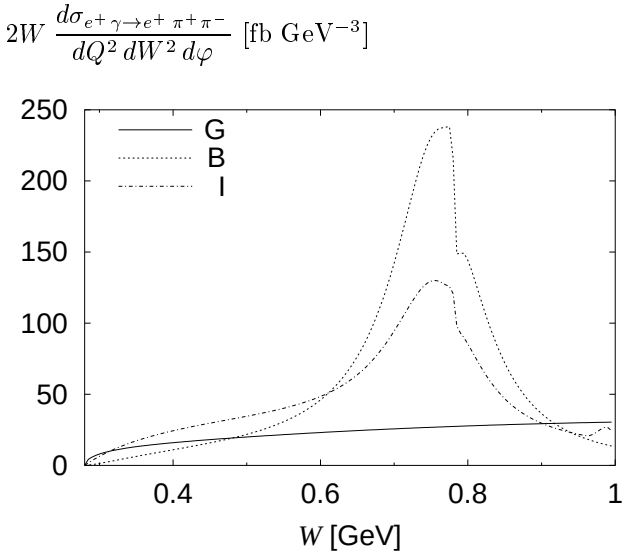

FIG. 14. The W-dependence of the different contributions to the differential $e^+\gamma$ cross section at $Q^2 = 5$ GeV^2, $\varphi = 0$ and $s_{e\gamma} = 50$ GeV^2. The corresponding values of y range from 0.1 to 0.12.

bremsstrahlung term should be flat, and the interference between them should be dominated by $\cos\varphi$ and $\cos 3\varphi$, going with A_{++} and A_{-+}, respectively. We show examples of the φ-behavior in Fig. 15, remembering that in our model A_{-+} is zero because we have neglected the contribution of the helicity-two gluon GDA. We notice that the $\cos 2\varphi$ term in bremsstrahlung, which is kinematically suppressed by $1 - x \sim W^2/Q^2$, is clearly visible at the larger energy $W = 800$ MeV. The θ-dependence, shown in Fig. 16, is also quite different for the three components of the cross section. For the $\gamma^*\gamma$ term and the interference it depends in detail on the coefficients of the different partial waves contributing to the amplitudes A_{ij}.

D. Studying the $\gamma^*\gamma$ subprocess through the interference term

The interference between the $\gamma^*\gamma$ and bremsstrahlung subprocesses provides an opportunity to study the $\gamma^*\gamma$ contribution at *amplitude* level. On one hand this means that one can completely separate the contributions A_{++}, A_{-+} and A_{0+} from different photon polarizations. On the other hand it gives access to the phases of these amplitudes relative to the phase of the pion form factor F_π, which is equal to the $\pi\pi$ phase shift δ_1 in the range of W we are considering. In kinematical regions where the bremsstrahlung amplitude is large, especially for W around the ρ mass peak, the interference can also be used to "amplify" the $\gamma^*\gamma$ signal.

For this to be useful it is essential that one can cleanly separate the interference term (90) from the pure $\gamma^*\gamma$ and bremsstrahlung contributions in the cross section. This is possible since the $\gamma^*\gamma$ collision produces the pion pair in the C-even channel, whereas in bremsstrahlung $\pi\pi$ occurs in the C-odd projection. The interference term can therefore be separated by reversing the charge of the lepton in the $e\gamma$ collision, a possibility that is automatically provided at e^+e^- colliders. Alternatively, any observable that is odd under exchange of the π^+ and π^- momenta is only sensitive to the interference term, which in turn drops out in any observable even under this exchange. In terms of the variables we are using, this exchange corresponds to the substitution $(\theta, \varphi) \to (\pi - \theta, \pi + \varphi)$. This means that we have direct access to the interference through the angular distribution of the pion pair in its rest frame. We emphasize that on the experimental level this does not require a perfect angular measurement, but only that the detection and reconstruction does not introduce a bias between positive and negative pions.

From the φ-dependence of the cross section one can extract the four coefficients C_n in Eq. (90), which determine the three quantities $\mathrm{Re}\{F_\pi^* A_{++}\}$, $\mathrm{Re}\{F_\pi^* A_{0+}\}$ and $\mathrm{Re}\{F_\pi^* A_{-+}\}$. In fact, they over-determine them, and one can for instance use only C_1, C_2, C_3, and keep the information from C_0 for a cross check. We remark in passing that this is owed to the fact that pions have zero spin, otherwise there would be more helicity amplitudes for the $\gamma^*\gamma$ reaction than independent observables one can extract from the φ-dependence. Using the φ-moments (86) with $m = 1, 2, 3$ and inverting the relation between C_1, C_2, C_3 and the helicity amplitudes we obtain

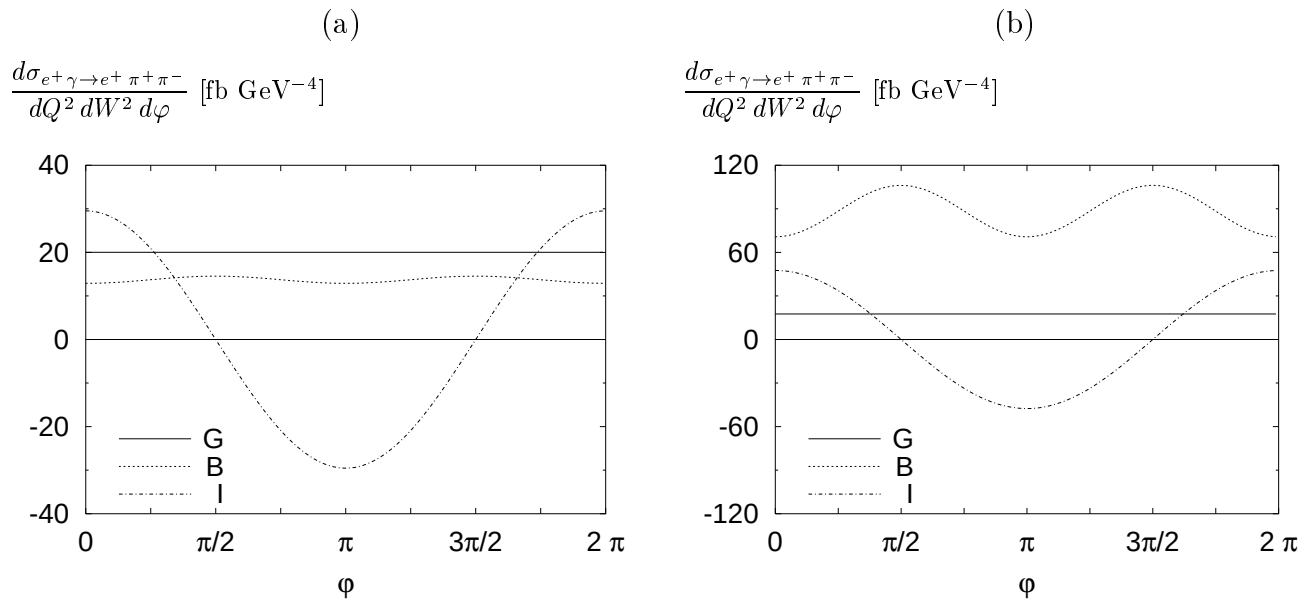

FIG. 15. (a) The φ-dependence of the different contributions to the differential $e^+\gamma$ cross section at $Q^2 = 5$ GeV^2, $W = 400$ MeV and $y = 0.1$. (b) The same for $W = 800$ MeV.

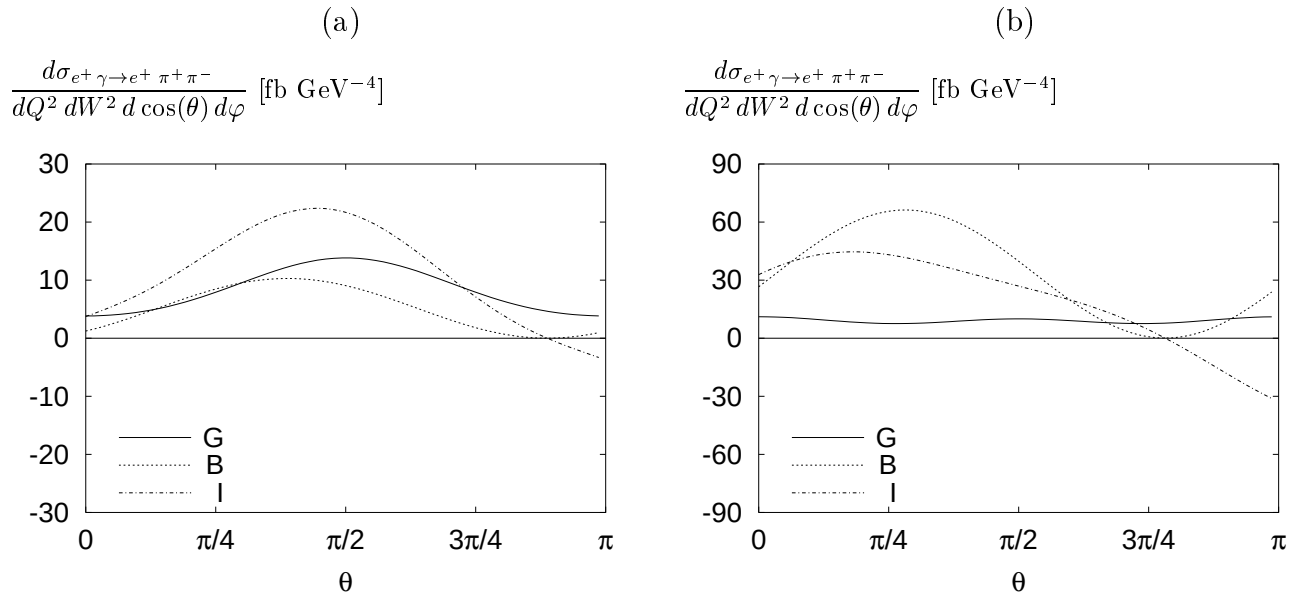

FIG. 16. (a) The θ-dependence of the different contributions to the differential $e^+\gamma$ cross section at $Q^2 = 5$ GeV^2, $W = 400$ MeV, $\varphi = 0$ and $y = 0.1$. (b) The same for $W = 800$ MeV.

$$\frac{K}{1-(1-x)(1+\epsilon)}\,\frac{dS_{e\gamma}(w_+)}{dQ^2\,dW^2\,d(\cos\theta)}+\Big\{\theta\leftrightarrow\pi-\theta\Big\}=2\,\mathrm{Re}\Big\{F_\pi^*A_{++}\Big\}\,\sin^3\theta,$$
$$\frac{K}{x\sqrt{\epsilon(1+\epsilon)}}\,\frac{dS_{e\gamma}(w_0)}{dQ^2\,dW^2\,d(\cos\theta)}+\Big\{\theta\leftrightarrow\pi-\theta\Big\}=2\,\mathrm{Re}\Big\{F_\pi^*A_{0+}\Big\}\,\sin^2\theta\cos\theta,$$
$$\frac{K}{x\epsilon}\,\frac{dS_{e\gamma}(w_-)}{dQ^2\,dW^2\,d(\cos\theta)}+\Big\{\theta\leftrightarrow\pi-\theta\Big\}=2\,\mathrm{Re}\Big\{F_\pi^*A_{-+}\Big\}\,\sin\theta \tag{93}$$

with a global factor

$$K(Q^2,W^2,\epsilon)=-e_l\left(\frac{\alpha^3}{8}\,\frac{(\beta xy)^2}{Q^4}\,\frac{\sqrt{2}}{\sqrt{W^2Q^2\epsilon(1-\epsilon)}}\right)^{-1} \tag{94}$$

and weights

$$\begin{aligned}
w_+ &= \sin^2\theta\cos\varphi-\sqrt{\frac{2(1-x)}{x}}\,\sqrt{\frac{\epsilon}{1+\epsilon}}\,2\cos\theta\sin\theta\cos2\varphi+\frac{1-x}{x\epsilon}\,(\sin^2\theta+4\epsilon\cos^2\theta)\cos3\varphi,\\
w_0 &= -\sin\theta\cos\theta\cos2\varphi+\sqrt{\frac{2(1-x)}{x}}\,\sqrt{\frac{1+\epsilon}{\epsilon}}\,\cos^2\theta\cos3\varphi,\\
w_- &= -\cos3\varphi.
\end{aligned} \tag{95}$$

By taking weights that are odd under the exchange of the π^+ and π^- momenta and summing over configurations with θ and $\pi-\theta$ we have canceled the contributions from the pure $\gamma^*\gamma$ and bremsstrahlung terms in the cross section. We remark that our method can easily be adapted to the case where one does not have full acceptance in φ, since the moments of $\cos\varphi$, $\cos2\varphi$ and $\cos3\varphi$ are always linear combinations of $\mathrm{Re}\{F_\pi^*A_{ij}\}$.

The functions w_i have been chosen such that they are finite, because the use of unbounded weighting functions is problematic. As a consequence, the terms $\mathrm{Re}\{F_\pi^*A_{ij}\}$ on the r.h.s. of Eq. (93) are still multiplied with functions of θ. One can avoid the rather strong suppression of angles θ near 0 or π in $\mathrm{Re}\{F_\pi^*A_{++}\}\sin^3\theta$ if the measurement of the moments (93) indicates that A_{-+} and A_{0+} are small compared with A_{++}. In this case one may replace the weight w_+ with $\cos\varphi$, whose moment is dominated by $A_{++}\sin\theta$ with corrections of order $\sqrt{1-x}\,A_{0+}$ and $(1-x)A_{-+}$. Alternatively, the moment of

$$w'_+=\sin\theta\cos\varphi-\sqrt{\frac{2(1-x)}{x}}\,\sqrt{\frac{\epsilon}{1+\epsilon}}\,2\cos\theta\cos2\varphi, \tag{96}$$

projects on $A_{++}\sin^2\theta$ with corrections only of order $(1-x)A_{-+}$. In a similar way the moment of $\cos\theta\cos2\varphi$ approximately projects on $A_{0+}\sin\theta\cos\theta$ if A_{-+} is sufficiently small.

The θ-dependence of the moments (93) contains information on the partial wave decomposition of the pion pair. One way to extract the partial waves is of course to fit the θ-dependence of the weighted differential cross sections (93). Alternatively, one can use weighted cross sections integrated over both φ and θ. The weight $\cos3\varphi\,P_l^2(\cos\theta)/\sin\theta$ readily projects out the lth partial wave in A_{-+} as we easily see from Eq. (93). Note that, since $P_l^2(\cos\theta)\propto\sin^2\theta$, this weighting function is a trigonometric polynomial. Similarly, $\cos2\varphi\,P_l^1(\cos\theta)/\sin\theta$ can be used to obtain the lth partial wave in A_{0+} if the contribution from A_{-+} is small enough.

For A_{++} the situation is more complicated, because the functions $w_+P_l(\cos\theta)/\sin^3\theta$, $w'_+P_l(\cos\theta)/\sin^2\theta$ and $\cos\varphi\,P_l(\cos\theta)/\sin\theta$ are all unbounded. The same problem occurs for the function $w_0\,P_l^1(\cos\theta)/(\sin^2\theta\cos\theta)$. In practice one may proceed as we discussed in Sect. VII B and restrict the analysis to a finite number of partial waves, which has to be determined from the data. Decomposing the coefficient C_n in (91) on polynomials $P_{l+1}^n(\cos\theta)$ one can see that if only partial waves with $l\le L$ are relevant in the amplitudes A_{ij}, then weighting the cross section with $\cos n\varphi\,P_{L+3}^n(\cos\theta)$ and integrating over φ and θ must give zero. For a restricted number of partial waves one can then find weights to project out the corresponding amplitudes. In the case where A_{-+} and A_{0+} are negligible and only the partial waves $l=0$ and $l=2$ are important in A_{++}, we have for instance

$$\frac{K}{1-(1-x)(1+\epsilon)}\,\frac{dS_{e\gamma}(w_{+l})}{dQ^2\,dW^2}=\mathrm{Re}\Big\{F_\pi^*A_{++l}\Big\},\qquad\qquad l=0,2 \tag{97}$$

with

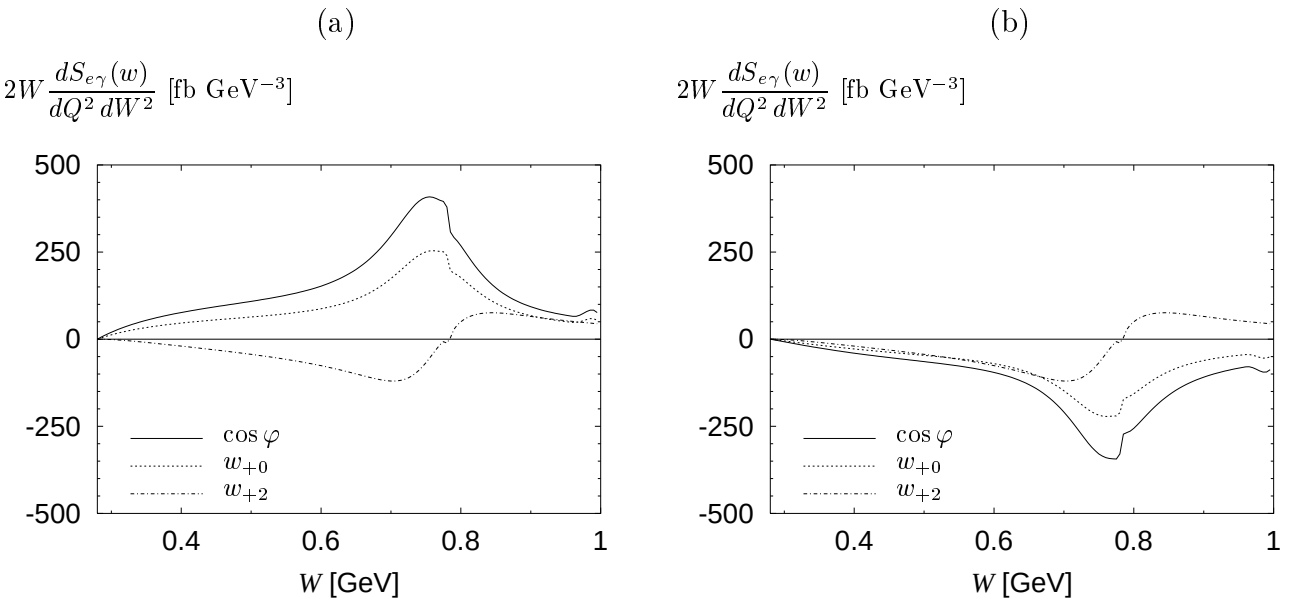

FIG. 17. (a) Differential cross sections weighted with $\cos\varphi$, w_{+0} and w_{+2}. The curves are calculated for an $e^+\gamma$ collision at $s_{e\gamma} = 50$ GeV^2 and $Q^2 = 5$ GeV^2 with the model GDA in (68). (b) The same for the alternative GDA described at the end of Sect. VII B.

$$w_{+0} = \frac{4}{3\pi}\,\cos\varphi\,(1 + 2\cos^2\theta), \qquad w_{+2} = -\frac{16}{3\pi}\,\cos\varphi\,(1 - 4\cos^2\theta). \tag{98}$$

In Fig. 17 we show the moments of $\cos\varphi$, w_{+0} and w_{+2} as a function of W for our model GDA (68) and also for the alternative ansatz described at the end of Sect. VII B. We clearly see the sensitivity of our observables to the detailed phase structure of the $\gamma^*\gamma$ amplitude.

E. Comparison with lepton pair production

In this section we compare our process $e\gamma \to e\,\pi^+\pi^-$ with the production of a muon pair, $e\gamma \to e\,\mu^+\mu^-$, in the same kinematics. This is interesting in itself because $\mu^+\mu^-$ production is the QED analogue of the reaction we are studying, but also because it constitutes an experimental background to the extent that a muon pair can be misidentified as a pair of charged pions.

The helicities of the muons can couple to 0 or ± 1 along the direction of the μ^+ momentum in the $\gamma^*\gamma$ c.m. From angular momentum conservation in the subprocesses $\gamma^*\gamma \to \mu^+\mu^-$ and $\gamma^* \to \mu^+\mu^-$ (the latter occurring in bremsstrahlung) it is clear that the dependence on θ and φ must be different in the cross sections for pion and for muon pair production. We therefore restrict ourselves here to the cross sections integrated over these angles. For the bremsstrahlung contribution we have

$$\left.\frac{d\sigma_{e\gamma\to eX}}{dQ^2\,dW^2}\right|_B = \frac{\alpha^3}{3s_{e\gamma}^2}\,\frac{1 - 2x(1-x)(1-\epsilon)}{\epsilon}\,f_B^X(W^2), \tag{99}$$

where

$$f_B^{\pi^+\pi^-} = \frac{\beta^3|F_\pi(W^2)|^2}{W^2}, \qquad f_B^{\mu^+\mu^-} = \frac{2\beta_\mu(3-\beta_\mu^2)}{W^2} \tag{100}$$

with the muon velocity $\beta_\mu = (1 - 4m_\mu^2/W^2)^{1/2}$ in the $\gamma^*\gamma$ c.m. For the $\gamma^*\gamma$ process we can easily adapt the result (73) for open $q\bar{q}$-production to the $\mu^+\mu^-$ case and find

$$\left.\frac{d\sigma_{e\gamma\to eX}}{dQ^2\,dW^2}\right|_G = \frac{\alpha^3}{4s_{e\gamma}^2}\,\frac{1}{Q^2(1-\epsilon)}\,f_G^X(W^2), \tag{101}$$

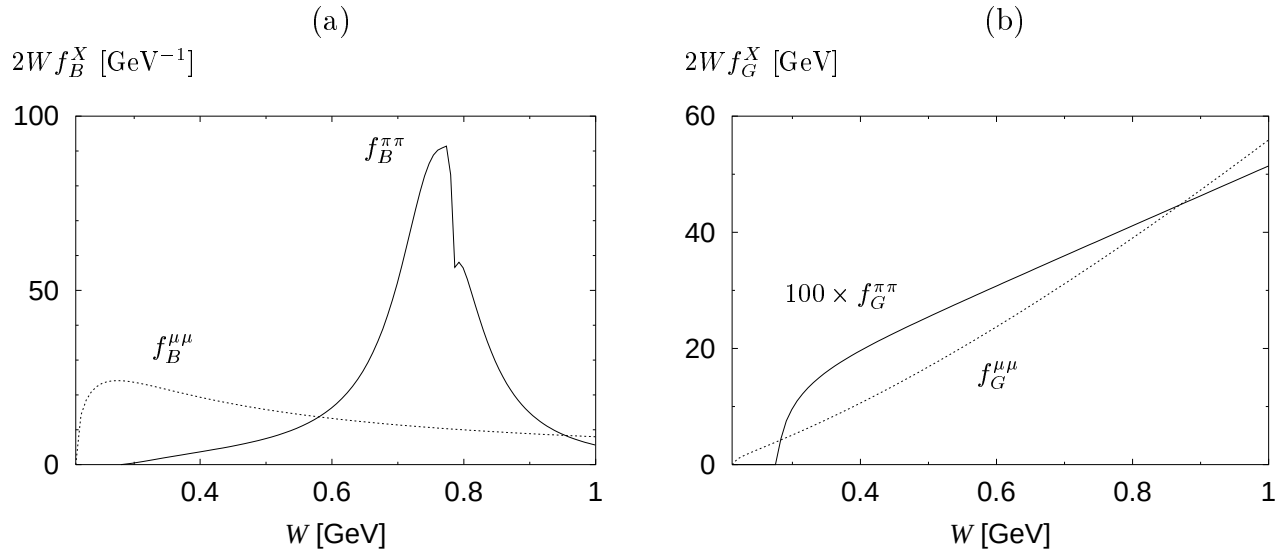

FIG. 18. (a) The functions f_B^X occurring in the bremsstrahlung contribution (99) to $\pi^+\pi^-$ and $\mu^+\mu^-$ production. They are plotted against W instead of W^2 and therefore have been multiplied with a Jacobian $2W$. (b) The same for the functions f_G^X in the $\gamma^*\gamma$ contribution (101). Note that the curve for pions, obtained with our model GDA (68), has been multiplied by a factor 100.

where

$$f_G^{\pi^+\pi^-} = \left(\frac{25R_\pi}{18}\right)^2 \beta\left(1 - \frac{2}{3}\beta^2 + \frac{1}{5}\beta^4\right), \qquad f_G^{\mu^+\mu^-} = 8\left(\ln\frac{1+\beta_\mu}{1-\beta_\mu} - \beta_\mu\right), \tag{102}$$

up to corrections of order W^2/Q^2. Notice that both for bremsstrahlung and for $\gamma^*\gamma$, the Q^2-dependence is the same in the pion and the muon case.

The functions f_B^X and f_G^X are compared in Fig. 18. We see that for the bremsstrahlung contribution pion production is enhanced by the strong resonance effect around the ρ mass, as manifested in $F_\pi(W^2)$. In the $\gamma^*\gamma$ subprocess, on the other hand, we find that with our estimate of the GDA, pion production is suppressed compared to muons by a factor 50 to 100. This is mostly due to the numerical constants in the expressions (102). In part it also comes from the logarithm $\log(1-\beta_\mu)$ in $f_G^{\mu^+\mu^-}$, which is generated by the collinear regions around $\theta = 0$ and π as discussed in Sect. VI. Notice that for this reason the $\mu^+\mu^-$ cross section will be relatively sensitive to cuts that affect θ. The same will apply to the interference between bremsstrahlung and $\gamma^*\gamma$, which drops of course out after angular integration. From the results on f_B^X and f_G^X we expect that the ratio of muon to pion pair production will be appreciable in the interference term.

Another experimental background, again due to particle misidentification, is $e^\pm\gamma \to e^\pm\, e^+e^-$. Compared with $\mu^+\mu^-$ production there are further Feynman diagrams, which can be obtained from the muon case by interchanging the lines with momenta k' and either p or p', now corresponding to identical particles. We shall not analyze these diagrams here, but will at least assess the contributions from those diagrams that are also present in muon production. Replacing β_μ with β_e we obtain velocities extremely close to 1. Nothing dramatic happens in the bremsstrahlung part (100), but the logarithm in the $\gamma^*\gamma$ subprocess (102) is now much larger than for muons. This large logarithm is however generated by transverse momenta $p_\perp$ of order m_e in the $\gamma^*\gamma$ c.m., which correspond to extremely small angles θ of order m_e/W. For any cut that effectively leads to a minimum angle θ_{min} much larger than that, one has to replace β_μ with $\cos\theta_{min}$ in Eq. (102), which can significantly reduce the size of the logarithm.

We finally note that the differential cross sections for $e^+e^- \to e^+e^-\, e^+e^-$ and $e^+e^- \to e^+e^-\, \mu^+\mu^-$ have been fully calculated to first order in QED and are available in the form of Monte Carlo generators [34].

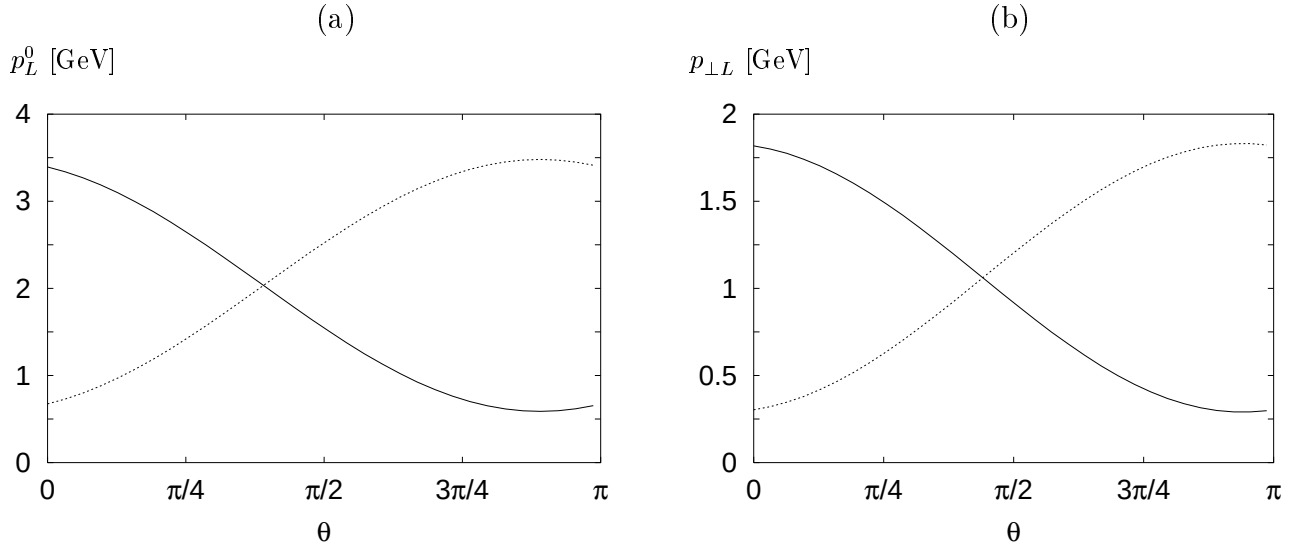

FIG. 19. (a) The pion energies p_L^0 (solid) and $p_L'^0$ (dotted) in the laboratory as a function of the angle θ in the two-pion c.m. The values of the remaining kinematical variables are $E_1 = 3.1$ GeV, $E_2 = 9$ GeV, $Q^2 = 5$ GeV^2, $W = 400$ MeV, $y = 0.1$, $\varphi = 0$. (b) The same for the transverse pion momenta $p_{\perp L}$ and $p'_{\perp L}$ in the laboratory.

VIII. CROSS SECTION ESTIMATES

A. Laboratory kinematics and experimental cuts

Before giving our estimates for the cross section of our process at various e^+e^- colliders, we give a brief discussion of the kinematics in the laboratory frame and the effects of some experimental cuts. Starting with the kinematics of the scattered lepton k', we remark that there is a simple transformation between the variables (Q^2, y) and $(E_1^{'}, \alpha_{1L})$, where $E_1^{'}$ and α_{1L} respectively are the energy and scattering angle of k' in the laboratory frame. Imposing minimum values on both quantities we have

$$y = 1 + \frac{Q^2}{4E_1^2} - \frac{E_1'}{E_1} \leq 1 + \frac{Q^2}{4E_1^2} - \frac{E_1'^{min}}{E_1} \tag{103}$$

and

$$y = 1 - \frac{Q^2}{4E_1^2}\frac{1+\cos\alpha_{1L}}{1-\cos\alpha_{1L}} \geq 1 - \frac{Q^2}{4E_1^2}\frac{1+\cos\alpha_{1L}^{min}}{1-\cos\alpha_{1L}^{min}}. \tag{104}$$

The condition (103) cuts on large values of y and is generally not very serious, because most information on the $\gamma^*\gamma$ process is obtained from low or intermediate y as we discussed after Eq. (92). The lower cut (104), on the other hand, severely restricts the interesting y-range in some experimental setups if Q^2 is not large enough. We will encounter an example of this in Sect. VIII B.

The transformation of the pion momenta into the laboratory system leads to rather lengthy expressions, which we will not give here. Notice that the lepton k' has a large transverse momentum $k'_{\perp L} = Q\sqrt{1-y}$ in the laboratory, which must be compensated by the two pions. Even though the $\pi\pi$ system has a rather low invariant mass, the pions thus carry large transverse momentum which helps to detect them. An exception are configurations with the the c.m. angle θ close to 0 or π, which in the laboratory correspond to an asymmetric sharing of momentum between the two pions. This is illustrated in Fig. 19.

It is instructive to consider the point where there the $\pi\pi$ system has zero longitudinal momentum P_L^3 in the laboratory. With the approximation $W^2 \ll Q^2$ we find

$$P_L^3 = yE_1 - \frac{1-y}{y}\frac{Q^2}{4E_1}, \tag{105}$$

so that $P_L^3 = 0$ when y equals

$$y_0 = \frac{Q}{2E_1}\left(\sqrt{1+\frac{Q^2}{16E_1^2}} - \frac{Q}{4E_1}\right). \tag{106}$$

For $Q \ll E_1$ this simplifies to $y_0 = Q/(2E_1)$. If y is very different from y_0 the $\pi\pi$ system is strongly boosted along the beam axis, and if this boost is too large then one or both pions will go out of the detector acceptance.

We finally have to discuss the kinematics of the scattered lepton l' in the laboratory. In terms of its scattering angle α_{2L} we have, up to electron mass corrections,

$$l'_{\perp L} = (1-x_2)\, E_2\, \sin\alpha_{2L} \tag{107}$$

for the transverse component of l', and

$$Q'^2 = -q'^2 = (1-x_2)\, E_2^2\, \left(2\sin\frac{\alpha_{2L}}{2}\right)^2 \tag{108}$$

for the photon virtuality. For small α_{2L} we obtain the simple relation

$$Q'^2 = \frac{l'^2_{\perp L}}{1-x_2}. \tag{109}$$

It turns out that an antitagging condition on the lepton l', i.e., $\alpha_{2L} \leq \alpha_{2L}^{max}$ with α_{2L}^{max} determined by the acceptance of a lepton in the detector, is not enough to keep Q'^2 small. With the parameters E_2 and α_{2L}^{max} in Tables I and III we find that, except in the region of x_2 very close to 1, the maximum values of Q'^2 and $l'^2_{\perp L}$ are a few GeV^2. Under such circumstances it is clearly inappropriate to approximate q'^2 as zero and the momenta l, l', q' as collinear, which we have done throughout this work. Both the kinematical transformation from the $e\gamma$ frame to the laboratory and the calculation of the cross section have to be modified then. For charged pion production one must not only recalculate the $\gamma^*\gamma$ and bremsstrahlung processes of Fig. 10 but also include the diagrams where the bremsstrahlung is not from the lepton k but from l. Although this is possible in principle, we wish to retain here the simpler expressions for the cross section with one real photon. We therefore require that Q'^2 be small compared with the other kinematical invariants in our problem.

A way to achieve this, suggested by Eq. (109), is to impose an upper cut on $l'_{\perp L}$, i.e., in practical terms on the sum $|\mathbf{k}'_{\perp L} + \mathbf{p}_{\perp L} + \mathbf{p}'_{\perp L}|$ of the reconstructed transverse momenta, possibly supplemented by a lower cut on $1-x_2$. In our numerical studies we determine the maximum virtuality Q'^2_{max} in the photon flux of Eq. (81) through Eqs. (107) and (108) by requiring both $\alpha_{2L} \leq \alpha_{2L}^{max}$ and $l'_{\perp L} \leq l'^{max}_{\perp L} = 100$ MeV. This leads to considerably smaller virtualities than the antitagging condition alone, although for x_2 very close to 1 the resulting Q'^2_{max} is still not very much smaller than W^2. In practice one may therefore consider an additional cut on x_2, but we have refrained from this in our estimates. Notice that the Q'^2-spectrum of the photon flux is logarithmic so that a substantial part of the cross section comes from Q'^2 much smaller than Q'^2_{max}.

B. B-factories

We have now all elements to give cross section estimates for existing e^+e^- facilities. We start with the B-factories, BABAR, BELLE and CLEO, running at a c.m. energy $\sqrt{s_{ee}}$ around 10 GeV. Using our model GDA (68) we calculate the integrated cross section σ and the individual contributions σ_G and σ_B from the $\gamma^*\gamma$ and bremsstrahlung subprocesses. To project out their interference term we take simple examples of weighted e^+e^- cross sections, $S_{ee}(\mathrm{sgn}(\cos\varphi))$ and $S_{ee}(\cos\varphi)$, defined in complete analogy with the weighted $e\gamma$ cross sections (83). We remark that $S_{ee}(\mathrm{sgn}(\cos\varphi))$ is simply the left-right asymmetry of the pions in their c.m. We integrate over y from its lower kinematical limit

$$y \geq \frac{Q^2+W^2}{4E_1E_2} \tag{110}$$

up to $y = 0.5$. Choosing a larger value increases the cross section, but the gain is mainly due to bremsstrahlung. Up to which values of y one can extract useful information on the $\gamma^*\gamma$ process depends of course on the detailed kinematics and must be studied in each particular case. The same is true for the upper limit of the Q^2-integration. For its lower limit we take 4 GeV^2 as a minimum value where one might expect a lowest-order calculation to be reliable, cf. our discussion in Sect. V. To determine the value of Q'^2_{max} in the equivalent photon flux we impose the cuts discussed at

	BABAR e^- tagged	BABAR e^+ tagged	BELLE e^- tagged	BELLE e^+ tagged	CLEO
E_1 [GeV]	9	3.1	8	3.5	5.3
E_2 [GeV]	3.1	9	3.5	8	5.3
α_{2L}^{max} [mrad]	684	300	154	112	227
σ [fb]	452	452	452	452	453
σ_G [fb]	15	15	14	15	15
σ_B [fb]	437	438	437	438	438
$S_{ee}(\mathrm{sgn}(\cos\varphi))$ [fb]	-51	52	-51	51	51
$S_{ee}(\cos\varphi)$ [fb]	-40	40	-40	40	41
$\sqrt{N}\,\delta(\mathrm{sgn}(\cos\varphi))$	8.8	8.8	8.8	8.8	8.8
$\sqrt{N}\,\delta(\cos\varphi)$	7.7	7.7	7.7	7.7	7.7

TABLE I. Cross sections for $e^+e^- \to e^+e^-\,\pi^+\pi^-$, integrated over the range $W = 300$ MeV to 1000 MeV, $Q^2 = 4$ GeV^2 to 20 GeV^2, and y from its lower kinematical limit (110) up to 0.5. The cut parameters α_{2L}^{max} and $l'^{max}_{\perp L} = 100$ MeV determine the real photon flux as described in Sect. VIII A. In the column for CLEO, the sign of the weighted cross sections $S_{ee}(\mathrm{sgn}(\cos\varphi))$ and $S_{ee}(\cos\varphi)$ corresponds to a tagged e^+.

	BABAR e^- tagged	BABAR e^+ tagged	BELLE e^- tagged	BELLE e^+ tagged	CLEO
α_{1L}^{min} [mrad]	300	684	112	154	227
$(\pi - \alpha_{1L}^{max})$ [mrad]	684	300	154	112	227
θ_L^{min} [mrad]	300	684	297	524	314
$(\pi - \theta_L^{max})$ [mrad]	684	300	524	297	314
σ [fb]	329	433	433	443	446
σ_G [fb]	6	12	13	13	14
σ_B [fb]	323	422	420	430	433
$S_{ee}(\mathrm{sgn}(\cos\varphi))$ [fb]	-31	48	-50	51	52
$S_{ee}(\cos\varphi)$ [fb]	-24	38	-39	40	41
$\sqrt{N}\,\delta(\mathrm{sgn}(\cos\varphi))$	10.5	8.9	8.7	8.7	8.6
$\sqrt{N}\,\delta(\cos\varphi)$	9.0	7.8	7.6	7.6	7.5

TABLE II. As Table I but with cuts imposed on the detection angles as specified, and in addition a minimum transverse momentum for the tagged lepton and for both pions of 100 MeV in the laboratory. E_1, E_2 and α_{2L}^{max} for each column are the same as in Table I.

the end of Sect. VIII A. Our results for $e^+e^- \to e^+e^-\,\pi^+\pi^-$ are given in Table I, where apart from the quantities just discussed we also give the coefficients in the relative statistical errors $\delta(w) \sim \mathrm{const}/\sqrt{N}$ of the weighted cross sections $S_{ee}(w)$. We see that the results for the different kinematical situations are practically identical. This indicates that it is the cut $l'_{\perp L} \leq 100$ MeV which determines the real photon flux in most of the relevant parameter space, and not the cut on α_{2L}, which is different in each of the five cases. We also find that $S_{ee}(\cos\varphi)$ has a slightly smaller relative statistical error than $S_{ee}(\mathrm{sgn}(\cos\varphi))$ and thus greater sensitivity to the interference term.

To estimate the effects of experimental acceptance for the detected particles we impose

- a cut $\alpha_{1L}^{min} \leq \alpha_{1L} \leq \alpha_{1L}^{max}$ on the scattering angle α_{1L} of the tagged lepton k',
- a cut $\theta_L^{min} \leq (\theta_L\,, \theta'_L) \leq \theta_L^{max}$ on the polar angles θ_L and θ'_L of the pion momenta p and p', measured with respect to the direction of the initial beam lepton k,
- a minimum transverse momentum of 100 MeV for the tagged lepton and for each of the pions.

All quantities refer of course to the laboratory frame. The results are shown in Table II.

Comparing with Table I we see that the effects of these cuts are generally quite moderate. The strongest effect is observed for BABAR kinematics in the case where the e^- is tagged. This can be traced back to the constraint $\alpha_{1L}^{min} \leq \alpha_{1L}$. The minimum value of y implied by Eq. (104) for $Q^2 = 4$ GeV^2 is 0.46 in this case, which effectively cuts away all phase space where the $\gamma^*\gamma$ process is relevant. The situation improves rapidly as Q^2 goes up, and for

	LEP1		LEP2	
	no cuts	with cuts	no cuts	with cuts
$E_1 = E_2$ [GeV]	45	45	95	95
Q^2_{max} [GeV^2]	20	20	40	40
σ [fb]	1023	167	1333	50
σ_G [fb]	86	53	124	17
σ_B [fb]	937	114	1209	33
$S_{ee}(\mathrm{sgn}(\cos\varphi))$ [fb]	128	41	159	13
$S_{ee}(\cos\varphi)$ [fb]	101	32	125	10
$\sqrt{N}\,\delta(\mathrm{sgn}(\cos\varphi))$	8.0	4.0	8.4	3.7
$\sqrt{N}\,\delta(\cos\varphi)$	7.0	3.5	7.4	3.3

TABLE III. Cross sections for $e^+e^- \to e^+e^-\,\pi^+\pi^-$, integrated over the range $W = 300$ MeV to 1000 MeV, $Q^2 = 4$ GeV^2 to Q^2_{max}, and y from its lower kinematical limit (110) up to 0.5. The columns marked "no cuts" correspond to imposing only the cuts that determine the real photon flux as explained in Sect. VIII A, with parameters $\alpha_{2L}^{max} = 30$ mrad and $l'^{max}_{\perp L} = 100$ MeV. The columns "with cuts" refer to the additional cuts described in the text. The sign of the weighted cross sections $S_{ee}(\mathrm{sgn}(\cos\varphi))$ and $S_{ee}(\cos\varphi)$ is for a tagged e^+.

$Q^2 = 6$ GeV^2 our cut implies $y \geq 0.19$. For the other experimental configurations the same cut is much less restrictive: for BABAR kinematics with a tagged e^+ our cut on α_{1L} implies $y \geq 0.18$ at $Q^2 = 4$ GeV^2, whereas in the cases of BELLE and CLEO there is not restriction on y from the inequality (104) at all, not even at $Q^2 = 4$ GeV^2.

We find that in the kinematics of B-factories the interference term is clearly larger than the contribution from $\gamma^*\gamma$ alone. With several 10 fb^{-1} integrated luminosity our estimated cross sections give event rates of order 10,000. As we see from the tables, the relative statistical error on the interference term, extracted through the moments $S_{ee}(\mathrm{sgn}(\cos\varphi))$ or $S_{ee}(\cos\varphi)$ is about 8 to 10 times larger than for integrated cross sections (where it is $1/\sqrt{N}$), so that the interference could be measured with statistical errors in the 10% range.

For the production of neutral pion pairs we easily obtain the cross section without cuts by multiplying σ_G in Table I with a factor 1/2, due to the restricted phase space of identical particles. We refrain from a discussion of the experimental reconstruction of the four-photon state coming from two pion decays, but for an order-of-magnitude indication of event rates one may take half of the cross sections σ_G in Table II. We then estimate hundreds of events with several 10 fb^{-1}, corresponding again to a statistical error around 10%. Thus studies of both charged and neutral pair production seem promising to us.

C. LEP

Let us now investigate the situation at high-energy colliders, taking as examples LEP1 at $E_1 = E_2 = 45$ GeV and LEP2 at $E_1 = E_2 = 95$ GeV.

In the columns labeled "no cuts" in Table III we list our predicted cross sections, with cuts only on $l'_{\perp L}$ and α_{2L} so that the real photon flux is defined. For the kinematics we have chosen, the cross sections come out about a factor 2 to 3 larger than at the B-factories. Luminosities at LEP are however much smaller, so that unfortunately we estimate rather low achievable event rates, and it is not clear to what extent studies of our process in this kinematical regime will be feasible.

To see the effect of cuts on the detected particles we require

- $\alpha_{1L}^{min} \leq \alpha_{1L} \leq \pi - \alpha_{1L}^{min}$ with $\alpha_{1L}^{min} = 30$ mrad and $E_1^{'} \geq 0.7\,E_1$ for the tagged lepton,
- $\theta_L^{min} \leq (\theta_L\,, \theta'_L) \leq \pi - \theta_L^{min}$ with $\theta_L^{min} = 262$ mrad, corresponding to pseudorapidities $|\eta| \leq 2$, and a minimum transverse momentum of 100 MeV for each of the pions.

The results are given in the columns "with cuts" of Table III. The most serious restriction here is the cut on the pion angles θ_L and θ'_L. This can be understood from our considerations after Eq. (106). The value of y where the $\pi\pi$ system has zero longitudinal momentum in the laboratory is $Q/(2E_1)$ and thus of order 0.01 to 0.05 here. Over most of the y-range the pions are therefore so strongly boosted in the lab that they appear under extremely small angles and cannot be detected. We observe in fact in Table III that the effect of cuts is stronger at LEP2 with its

higher beam energy, and that it is more pronounced for bremsstrahlung than for the $\gamma^*\gamma$ process, the latter being less affected by a loss of events at larger y.

At LEP1 the cut on α_{1L} puts no restriction on y, but for LEP2 we find that for $Q^2 = 4$ GeV^2 it implies $y > 0.5$, so that one must go to larger Q^2. For Q^2 of about 8 GeV^2 there is no restriction on y from the constraint (104) any more.

We finally note that at the very large values of Q^2 accessible at high-energy colliders one can afford invariant masses W well above 1 GeV, while still fulfilling the basic condition $W^2 \ll Q^2$ of our study. We have not explored this mass region, since our model for the pion GDA is not applicable there. It is however clear that there will be a strong enhancement of the GDAs at W around the masses of C-even resonances, such as the $f_2(1270)$.

IX. SUMMARY AND OUTLOOK

In this paper we have analyzed in detail the process $\gamma^*\gamma \to \pi\pi$ in the domain where the virtuality Q of the γ^* is much larger than the invariant mass W of the two-pion system. It factorizes into a parton-level subprocess, which is under perturbative control, and non-perturbative matrix elements called generalized distribution amplitudes. This makes the reaction a laboratory to study the non-perturbative dynamics of a two-pion system forming from a well-defined partonic state, namely from a quark-antiquark or a two-gluon pair produced at small distance. The perturbative stage of the overall process is completely analogous to the one in single-meson production, well studied in the case of a π^0, η and η'. It results in a scaling behavior of the amplitude as Q^2 increases at fixed W^2, selects characteristic helicity combinations of the two photons, and predicts that the two pions are produced with total isospin zero. The dynamical content of the non-perturbative matrix elements, on the other hand, is more complex than for a single particle. Even the lowest Fock state of $|\pi\rangle \otimes |\pi\rangle$, that is, $q\bar{q} \otimes q\bar{q}$, contains more partons that the initial $q\bar{q}$ or gg system from which the two pions are formed. In this sense a GDA describes the transition between different parton configurations in the non-perturbative regime. The two-pion distribution amplitude contains the full strong interactions between the two pions, leading to dynamical phases which, by Watson's theorem, are identical to the phase shifts in elastic $\pi\pi$ scattering as long as W is below the inelastic threshold. We use this relation as an input for our model GDA, and therefore restrict our study to the W-region up to 1 GeV.

The evolution equation giving the factorization scale dependence of the GDAs is more complex than for a single pion due to the mixing of $q\bar{q}$ or gg amplitudes, and we have given the relevant splitting functions and anomalous dimensions for the quantum numbers of relevance here. A simultaneous expansion of $\Phi(z, \zeta, W^2)$ in the parton momentum fraction z and partial waves of the pion system leads to local matrix elements between the vacuum and a two-pion state. By analytic continuation they are related to the moments of the parton distribution functions of the pion. We have used the quark momentum fraction R_π in the pion, determined from a global fit of these distributions, as an input for our model of $\Phi(z, \zeta, W^2)$. The corresponding value of R_π is well below its asymptotic value under perturbative evolution, which may be an indication that the lowest non-asymptotic terms in the crossed-channel quantity $\Phi(z, \zeta, W^2)$ are not small at factorization scales in the GeV range. We emphasize that the question of how close one is to the asymptotic result of evolution is particularly interesting, because in the case of light pseudoscalars the single-meson distribution amplitudes may be surprisingly close to their asymptotic form even at low scales [9,30].

From a theory point of view it is also interesting to consider $\Phi_q(z, \zeta, W^2)$, defined by the matrix element in Eq. (13), for values of W much larger than the scale of non-perturbative interactions. While the dynamics in $\Phi_q(z, \zeta, W^2)$ is entirely soft for small W, part of it becomes hard when W increases. In the limit $W \gg 1$ GeV and to leading order in α_S one can explicitly write $\Phi_q(z, \zeta, W^2)$ in terms of a perturbative subprocess and the $q\bar{q}$ distribution amplitudes for each separate pion [35]. The resulting $\Phi_q(z, \zeta, W^2)$ is very far from the asymptotic form in z. It receives substantial contributions from high partial waves of the $\pi\pi$ system, has a power-law falloff like $1/W^2$, and its imaginary part is small compared to its real part.

We have constructed a model for the GDA at W below 1 GeV, using simple structure as a guide, and R_π and the $\pi\pi$ phase shifts as phenomenological inputs. Comparing the rates for the production of $\pi\pi$ and of a single pseudoscalar meson, we found that the hadron spectrum in $\gamma^*\gamma$ collisions below 1 GeV is strongly dominated by the single resonances π^0, η, and η'.

We have further compared our process with open $q\bar{q}$ production, which at higher invariant masses W is commonly used to describe the part of the total hadronic $\gamma^*\gamma$ cross section due to the pointlike part of the real photon. Interestingly, we find that in our particular kinematical limit, the corresponding scattering amplitude has the same scaling behavior and helicity structure as the one for the exclusive processes $\gamma^*\gamma \to \pi$ and $\gamma^*\gamma \to \pi\pi$. The main difference is that in the π and $\pi\pi$ cases the collinear divergence of the lowest-order hard scattering diagrams is regulated by the hadronization process. This is encapsulated in the distribution amplitudes, which vanish at the end points $z = 0$ and 1. In the open $q\bar{q}$ calculation, on the other hand, the divergence has to be regulated explicitly. We also note that the

sensitivity to the soft end-point region may be larger for pion-pair production than for a single pion, because for two pions the hard scattering and the distribution amplitudes vanish at $z = 1/2$ for symmetry reasons. Thus one may expect the onset of the scaling behavior to occur at different Q^2 in the two cases, an issue that will be interesting to study in experiment.

An investigation of the structure of the cross section shows that in $e\gamma$ and e^+e^- collisions information on the $\gamma^*\gamma$ process can be obtained either through the square of the $\gamma^*\gamma$ amplitude, or from its interference with the bremsstrahlung process if the pions are charged. This interference can readily be projected out by appropriate C-odd observables, and it offers the opportunity to separate the different $\gamma^*\gamma$ helicity amplitudes. It further provides direct access to their dynamical phases, although a full phase reconstruction requires polarized beams (cf. Appendix B).

The angular distribution of the pion pair in its c.m. contains detailed information about the dynamics of the $\gamma^*\gamma$ process. The dependence on the azimuth φ separates the different helicity combinations of the real and virtual photon, each of which plays a distinct role in the scaling limit. In particular it permits one to study leading-twist and non-leading twist amplitudes at the same time, which should provide additional insight into how far one is from the asymptotic regime. The θ-dependence, on the other hand, gives access to the partial waves in which the two pions are produced. It is sensitive to the phases, which reflect the dynamics of the $\pi\pi$ system and its resonances. Even though one will probably not be able to perform a full extraction of the $\pi\pi$ phase shifts in this way, our process provides constraints on these quantities that are independent of the analyses of elastic $\pi\pi$ scattering. The presence of higher partial waves would in itself be very interesting, since it gives indirect information on the deviation of $\Phi(z, \zeta, W^2)$ from its asymptotic form in z.

We have restricted ourselves to the production of pion pairs in this work, but it is clear that many of our results are also valid for other exclusive systems. The most obvious generalization is to charged or neutral $K\bar{K}$ pairs, whose comparison with $\pi\pi$ would allow one to study aspects of flavor $SU(3)$ breaking in the context of the quark-hadron transition. At even higher values of W^2 there is the production of $p\bar{p}$, where extra spin degrees of freedom come in, as in the well-studied case of the parton distributions of the nucleon.

Another very similar process is the production of $\mu^+\mu^-$ pairs, i.e., the QED analogue of our reaction. Comparing the rates of $e\gamma \to e\,\mu^+\mu^-$ with our estimate for $e\gamma \to e\,\pi^+\pi^-$ we find that the bremsstrahlung mechanism prefers pions if W is in the vicinity of the ρ mass, reflecting the strong resonance effect in the $\pi\pi$ system. For the production from $\gamma^*\gamma$, on the other hand, the cross section is considerably larger in the case of muon pairs. We remark that this could not be anticipated from a dimensional analysis. The amplitudes for $\gamma^*\gamma \to \mu\mu$ and for $\gamma^*\gamma \to \pi\pi$ have the same Q^2-dependence in our kinematical limit, and the two-pion distribution amplitude, which describes that pions are not pointlike but have internal structure, is a dimensionless quantity.

Using our model GDA to calculate the cross section for $e^+e^- \to e^+e^-\,\pi\pi$, we find encouraging rates for the kinematics and luminosity of B-factories. Thus there should be enough statistics for detailed studies at these facilities. Our estimates of the effect of cuts also indicate that in the kinematical region interesting in our context, the pions and the tagged lepton are well within the experimental acceptance. For high-energy colliders such as LEP, our predictions are less optimistic, at least in the range of W below 1 GeV which we have studied here, due both to the lesser luminosity and the strong longitudinal boost of the pion system.

In conclusion, we find that the process $\gamma^*\gamma \to \pi\pi$ can offer valuable insight into the interactions between quarks, gluons and hadrons, and that it should well be measurable at existing e^+e^- facilities.

ACKNOWLEDGMENTS

It is a pleasure to thank P. Aurenche, S.J. Brodsky, T. Feldmann, M. Fontannaz, P. Hoyer, O. Nachtmann, M. Polyakov and O.V. Teryaev for discussions, and H. Marsiske, C. Munger, V. Savinov, S. Söldner-Rembold, S. Uehara and M. Wang for their interest and valuable information about experimental aspects.

M.D. thanks CPhT and LPNHE of École Polytechnique for kind invitations.

APPENDIX A: PION ISOSPIN STATES

We specify in this appendix our sign convention for the definition of pion states. The relative sign for π^+ and π^- is relevant because it determines the relative sign of the GDAs for charged and neutral pion pairs.

In terms of eigenstates $|\pi^i\rangle$ of the isospin operators I^i $(i = 1, 2, 3)$ we define

$$|\pi^+\rangle = \frac{1}{\sqrt{2}}\left(|\pi^1\rangle + i|\pi^2\rangle\right), \qquad |\pi^-\rangle = \frac{1}{\sqrt{2}}\left(|\pi^1\rangle - i|\pi^2\rangle\right), \qquad |\pi^0\rangle = |\pi^3\rangle. \tag{A1}$$

Notice that the sign for $|\pi^+\rangle$ is opposite to the usual convention for eigenstates of $SU(2)$. This has to be remembered when writing down two-pion states with definite isospin using the Clebsch-Gordan coefficients.

The convention (A1) is in line with the customs of field theory, see for instance Sect. 12.5 of [36]. If, starting from the real scalar fields associated with $|\pi^1\rangle$ and $|\pi^2\rangle$, one constructs the complex scalar field φ which creates $|\pi^-\rangle$ out of the vacuum, then $|\pi^+\rangle$ is created by the conjugated field φ^*. If one used the opposite sign in defining $|\pi^+\rangle$, which is more natural in the context of isospin, then there would be an extra minus sign between the fields creating $|\pi^-\rangle$ and $|\pi^+\rangle$. Through the LSZ reduction formula this sign would show up in crossing relations. With our definition (A1) this does not happen, and we have for instance that the spacelike pion form factor

$$\langle \pi^+(p)|\, J^\mu_{\rm em}(0)\, |\pi^+(p')\rangle = (p+p')^\mu\, F_\pi(t) \tag{A2}$$

with $t=(p-p')^2$ becomes

$$\langle \pi^+(p)\pi^-(p')|\, J^\mu_{\rm em}(0)\, |0\rangle = (p-p')^\mu\, F_\pi(s) \tag{A3}$$

with $s=(p+p')^2$ in the timelike region. We remark in passing that if one uses the isospin relation (22) and neglects the contributions from strange and heavy quarks, one has the sum rule

$$\int dz\, \Phi_u^-(z,\zeta,W^2) = (2\zeta-1)\, F_\pi(W^2). \tag{A4}$$

The choice (A1) also leads to a convenient relation for the action of the charge conjugation operator C, namely

$$C|\pi^+\rangle = |\pi^-\rangle, \qquad C|\pi^0\rangle = |\pi^0\rangle. \tag{A5}$$

The impossibility to find a sign convention that is natural for both charge conjugation and the isospin algebra is discussed at length in Chapt. 5, §7 of [37] (where the other sign in defining $|\pi^+\rangle$ was chosen). We also remark that the definition (A1) implies

$$\langle \pi^+|\, \bar u_\alpha(x)\, d_\beta(0)\, |0\rangle = \langle \pi^-|\, \bar d_\alpha(x)\, u_\beta(0)\, |0\rangle, \tag{A6}$$

and therefore a relative plus sign between the distribution amplitudes for π^+ and π^-.

Our definition is the same as the one chosen by Polyakov et al., cf. [18], and it was also adopted in [35]. We finally mention that the definition leading to Eq. (15) of [4] has the opposite sign for $|\pi^+\rangle$.

APPENDIX B: BEAM POLARIZATION

As we have shown in Sects. VII B and VII D, the unpolarized $e\gamma$ cross section contains detailed information on the $\gamma^*\gamma$ helicity amplitudes A_{ij}. From Eqs. (80) and (91) it is however clear that this information is not sufficient to fully reconstruct the three independent complex amplitudes A_{++}, A_{0+} and A_{+-}. For completeness we give in this appendix the expressions of the cross section with longitudinally polarized lepton and photon beams, and discuss what additional information can be obtained from single and double polarization asymmetries.

Starting with the $\gamma^*\gamma$ contribution, we have

$$\begin{aligned}
\left.\frac{d\sigma_{e\gamma\to e\,\pi\pi}}{dQ^2\,dW^2\,d(\cos\theta)\,d\varphi}\right|_G = \text{eq. (80)} + \frac{\alpha^3}{16\pi}\frac{\beta}{s_{e\gamma}^2}\frac{1}{Q^2(1-\epsilon)}\,\Big(\; & P_l\,\sin\varphi\,\mathrm{Im}\left\{A^*_{++}A_{0+} - A^*_{-+}A_{0+}\right\} 2\sqrt{\epsilon(1-\epsilon)} \\
& + P_\gamma\,\sin\varphi\,\mathrm{Im}\left\{A^*_{++}A_{0+} + A^*_{-+}A_{0+}\right\} 2\sqrt{\epsilon(1+\epsilon)} \\
& + P_\gamma\,\sin 2\varphi\,\mathrm{Im}\left\{A^*_{++}A_{-+}\right\} 2\epsilon \\
& + P_l P_\gamma\,\left\{|A_{++}|^2 - |A_{-+}|^2\right\}\sqrt{1-\epsilon^2} \\
& - P_l P_\gamma\,\cos\varphi\,\mathrm{Re}\left\{A^*_{++}A_{0+} + A^*_{-+}A_{0+}\right\} 2\sqrt{\epsilon(1-\epsilon)}\,\Big),
\end{aligned} \tag{B1}$$

where P_l and P_γ respectively denote the longitudinal polarization of the lepton and photon beam, ranging from -1 to 1. Together with Eq. (80) we see that if both lepton and photon are polarized, one has enough independent terms to reconstruct the real and imaginary parts of the interferences $A^*_{++}A_{-+}$, $A^*_{++}A_{0+}$ and $A^*_{-+}A_{0+}$. Furthermore, the

squared terms $|A_{++}|^2$ and $|A_{-+}|^2$ come with a different relative sign in the unpolarized cross section and the double polarization asymmetry.

The bremsstrahlung contribution to the cross section reads

$$\left.\frac{d\sigma_{e\gamma\to e\,\pi\pi}}{dQ^2\,dW^2\,d(\cos\theta)\,d\varphi}\right|_B = \text{eq. (89)} + \frac{\alpha^3}{16\pi}\,\frac{\beta}{s_{e\gamma}^2}\,\frac{2\beta^2}{W^2\,\epsilon}\,|F_\pi(W^2)|^2\,P_l P_\gamma\,\Big(\,(2x-1)\sqrt{1-\epsilon^2}\,\sin^2\theta + \cos\varphi\,\sqrt{2x(1-x)}\sqrt{\epsilon(1-\epsilon)}\,2\sin\theta\cos\theta\Big). \quad \text{(B2)}$$

Notice that it only contributes to the unpolarized cross section and the double polarization asymmetry, but not to single polarization asymmetries. Finally, the interference term can be written as

$$\left.\frac{d\sigma_{e\gamma\to e\,\pi\pi}}{dQ^2\,dW^2\,d(\cos\theta)\,d\varphi}\right|_I = \text{eq. (90)} - 2e_l\,\frac{\alpha^3}{16\pi}\,\frac{\beta}{s_{e\gamma}^2}\,\frac{\sqrt{2}\beta}{\sqrt{W^2Q^2\epsilon(1-\epsilon)}}\,\Big[\,P_l\left(C_1^l\,\sin\varphi + C_2^l\sin 2\varphi\right) + P_\gamma\left(C_1^\gamma\,\sin\varphi + C_2^\gamma\,\sin 2\varphi + C_3^\gamma\,\sin 3\varphi\right) + P_l\,P_\gamma\left(C_0^{l\gamma} + C_1^{l\gamma}\,\cos\varphi + C_2^{l\gamma}\,\cos 2\varphi\right)\Big] \quad \text{(B3)}$$

with coefficients

$$\begin{aligned}
C_1^l &= -\mathrm{Im}\Big\{F_\pi^* A_{++}\Big\}\,x\sqrt{1-\epsilon^2}\,\sin\theta \\
&\quad +\mathrm{Im}\Big\{F_\pi^* A_{-+}\Big\}\,(1-x)\sqrt{1-\epsilon^2}\,\sin\theta, \\
C_2^l &= \mathrm{Im}\Big\{F_\pi^* A_{0+}\Big\}\,x\sqrt{\epsilon(1-\epsilon)}\,\sin\theta \\
&\quad -\mathrm{Im}\Big\{F_\pi^* A_{-+}\Big\}\,\sqrt{2x(1-x)}\sqrt{\epsilon(1-\epsilon)}\,\cos\theta
\end{aligned} \quad \text{(B4)}$$

for lepton polarization,

$$\begin{aligned}
C_1^\gamma &= -\mathrm{Im}\Big\{F_\pi^* A_{++}\Big\}\,[1-(1-x)(1-\epsilon)]\,\sin\theta \\
&\quad +\mathrm{Im}\Big\{F_\pi^* A_{0+}\Big\}\,\sqrt{2x(1-x)}\,2\epsilon\,\cos\theta \\
&\quad -\mathrm{Im}\Big\{F_\pi^* A_{-+}\Big\}\,(1-x)\,\sin\theta \\
C_2^\gamma &= \mathrm{Im}\Big\{F_\pi^* A_{0+}\Big\}\,x\sqrt{\epsilon(1+\epsilon)}\,\sin\theta \\
&\quad +\mathrm{Im}\Big\{F_\pi^* A_{-+}\Big\}\,\sqrt{2x(1-x)}\sqrt{\epsilon(1+\epsilon)}\,\cos\theta, \\
C_3^\gamma &= \mathrm{Im}\Big\{F_\pi^* A_{-+}\Big\}\,x\epsilon\,\sin\theta
\end{aligned} \quad \text{(B5)}$$

for photon polarization, and

$$\begin{aligned}
C_0^{l\gamma} &= \mathrm{Re}\Big\{F_\pi^* A_{++}\Big\}\,\sqrt{2x(1-x)}\sqrt{\epsilon(1-\epsilon)}\,\cos\theta \\
&\quad -\mathrm{Re}\Big\{F_\pi^* A_{0+}\Big\}\,(1-x)\sqrt{\epsilon(1-\epsilon)}\,\sin\theta, \\
C_1^{l\gamma} &= \mathrm{Re}\Big\{F_\pi^* A_{++}\Big\}\,x\sqrt{1-\epsilon^2}\,\sin\theta \\
&\quad -\mathrm{Re}\Big\{F_\pi^* A_{-+}\Big\}\,(1-x)\sqrt{1-\epsilon^2}\,\sin\theta, \\
C_2^{l\gamma} &= -\mathrm{Re}\Big\{F_\pi^* A_{0+}\Big\}\,x\sqrt{\epsilon(1-\epsilon)}\,\sin\theta \\
&\quad +\mathrm{Re}\Big\{F_\pi^* A_{-+}\Big\}\,\sqrt{2x(1-x)}\sqrt{\epsilon(1-\epsilon)}\,\cos\theta
\end{aligned} \quad \text{(B6)}$$

if both lepton and photon are polarized. We see that with polarized photons one can extract $\mathrm{Im}\{F_\pi^* A_{++}\}$, $\mathrm{Im}\{F_\pi^* A_{0+}\}$ and $\mathrm{Im}\{F_\pi^* A_{-+}\}$, which together with the unpolarized interference term makes it possible to reconstruct all three

complex $\gamma^*\gamma$ amplitudes for values of W where the pion form factor F_π is known. One cannot achieve the same with a polarized lepton beam alone, since there are only two terms in the φ-dependence. In this case one can still use the suppression by $1-x$ of the second term in C_1^l in order to approximately extract $\mathrm{Im}\{F_\pi^* A_{++}\}$. Finally, the double polarization asymmetry gives access to the same quantities one can already obtain in the unpolarized case.

---

[1] H. Terazawa, Rev. Mod. Phys. **45**, 615 (1973).
[2] V.M. Budnev *et al.*, Phys. Rept. **15C**, 181 (1975).
[3] S.J. Brodsky, hep-ph/9708345, talk presented at PHOTON 97, Egmond aan Zee, Netherlands, May 1997;
M.R. Pennington, Nucl. Phys. **B** (Proc. Suppl.) **82**, 291 (2000), hep-ph/9907353.
[4] M. Diehl, T. Gousset, B. Pire and O.V. Teryaev, Phys. Rev. Lett. **81**, 1782 (1998), hep-ph/9805380;
M. Diehl, T. Gousset and B. Pire, Nucl. Phys. **B** (Proc. Suppl.) **82**, 322 (2000), hep-ph/9907453.
[5] D. Müller *et al.*, Fortschr. Phys. **42**, 101 (1994), hep-ph/9812448.
[6] A. Freund, Phys. Rev. **D61**, 074010 (2000), hep-ph/9903489.
[7] G.P. Lepage and S.J. Brodsky, Phys. Rev. **D22**, 2157 (1980).
[8] S. Ong, Phys. Rev. **D52**, 3111 (1995);
R. Jakob, P. Kroll and M. Raulfs, J. Phys. **G22**, 45 (1996), hep-ph/9410304;
P. Kroll and M. Raulfs, Phys. Lett. **B387**, 848 (1996), hep-ph/9605264;
A.V. Radyushkin and R.T. Ruskov, Nucl. Phys. **B481**, 625 (1996), hep-ph/9603408;
I.V. Musatov and A.V. Radyushkin, Phys. Rev. **D56**, 2713 (1997), hep-ph/9702443.
[9] CLEO Collab., J. Gronberg *et al.*, Phys. Rev. **D57**, 33 (1998), hep-ex/9707031.
[10] X. Ji, J. Phys. **G24**, 1181 (1998), hep-ph/9807358, and references therein.
[11] M. Diehl, T. Gousset and B. Pire, to appear in the Procs. of the Workshop on Exclusive and Semiexclusive Processes at High Momentum Transfer, Jefferson Lab, Newport News, VA, USA, May 1999, hep-ph/9909445;
B. Lehmann-Dronke *et al.*, hep-ph/9910310.
[12] K. Watanabe, Prog. Theor. Phys. **67**, 1834 (1982).
[13] J. Blümlein, B. Geyer and D. Robaschik, Nucl. Phys. **B560**, 283 (1999), hep-ph/9903520, and references therein.
[14] M. Diehl, T. Gousset, B. Pire and J.P. Ralston, Phys. Lett. **B411**, 193 (1997), hep-ph/9706344.
[15] J.C. Collins and M. Diehl, hep-ph/9907498, to appear in Phys. Rev. **D**.
[16] N. Kivel, L. Mankiewicz and M.V. Polyakov, Phys. Lett. **B467**, 263 (1999), hep-ph/9908334.
[17] V.N. Baier and A.G. Grozin, Nucl. Phys. **B192**, 476 (1981).
[18] M.V. Polyakov and C. Weiss, Phys. Rev. **D60**, 114017 (1999), hep-ph/9902451.
[19] M.V. Polyakov, Nucl. Phys. **B555**, 231 (1999), hep-ph/9809483.
[20] M.V. Polyakov, private communication.
[21] I.I. Balitsky and V.M. Braun, Nucl. Phys. **B311**, 541 (1988/89).
[22] G.P. Lepage and S.J. Brodsky, Phys. Lett. **B87**, 359 (1979);
A.V. Efremov and A.V. Radyushkin, Phys. Lett. **B94**, 245 (1980).
[23] M.K. Chase, Nucl. Phys. **B174**, 109 (1980).
[24] V.L. Chernyak and A.R. Zhitnitsky, Phys. Rept. **112**, 173 (1984).
[25] G. Altarelli, Phys. Rept. **81**, 1 (1982).
[26] P. Estabrooks and A.D. Martin, Nucl. Phys. **B79**, 301 (1974).
[27] B. Hyams *et al.*, Nucl. Phys. **B64**, 134 (1973);
D.V. Bugg, B.S. Zou and A.V. Sarantsev, Nucl. Phys. **B471**, 59 (1996);
R. Kaminski, L. Lesniak and K. Rybicki, hep-ph/9912354.
[28] J.H. Kühn and A. Santamaria, Z. Phys. **C48**, 445 (1990).
[29] M. Glück, E. Reya and I. Schienbein, Eur. Phys. J. **C10**, 313 (1999), hep-ph/9903288.
[30] T. Feldmann, Int. J. Mod. Phys. **A15**, 159 (2000), hep-ph/9907491.
[31] L.E. Gordon and J.K. Storrow, Z. Phys. **C56**, 307 (1992).
[32] M. Diehl and O. Nachtmann, Z. Phys. **C62**, 397 (1994).
[33] L.M. Barkov *et al.*, Nucl. Phys. **B256**, 365 (1985).
[34] F.A. Berends, P.H. Daverveldt and R. Kleiss, Nucl. Phys. **B253**, 441 (1985);
Comput. Phys. Commun. **40**, 285 (1986); Comput. Phys. Commun. **40**, 309 (1986).
[35] M. Diehl, T. Feldmann, P. Kroll and C. Vogt, Phys. Rev. **D61**, 074029 (2000), hep-ph/9912364.
[36] J.D. Bjorken and S.D. Drell, *Relativistic Quantum Fields*, McGraw-Hill, 1965.
[37] A.D. Martin and T.D. Spearman, *Elementary Particle Theory*, North Holland, 1970.